135900-2-F$_2$

Final Report

DETECTION OF BATHYMETRIC FEATURES USING SEASAT SYNTHETIC APERTURE RADAR - A FEASIBILITY STUDY

E.S. KASISCHKE, R.A. SHUCHMAN AND J.D. LYDEN

APRIL 1980

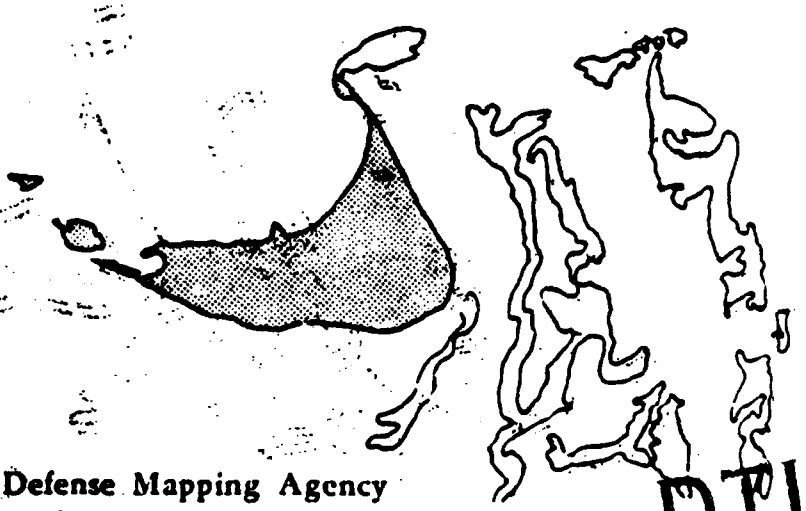

Defense Mapping Agency
Hydrographic/Topographic Center
Washington, D.C. 20315

Contract DMA 800-78-C-0060
Technical Monitor: James Hammack
Advanced Technology Division
Systems and Techniques Directorate

ENVIRONMENTAL
RESEARCH INSTITUTE OF MICHIGAN
BOX 8618 • ANN ARBOR • MICHIGAN 48107

TECHNICAL REPORT STANDARD TITLE PAGE

1. Report No.	2. Government Accession No.	3. Recipient's Catalog No.
135900-2-F_2		

4. Title and Subtitle	5. Report Date
Detection of Bathymetric Features Using SEASAT Synthetic Aperture Radar-A Feasibility Study	30 April 1980
	6. Performing Organization Code
7. Author(s)	8. Performing Organization Report No.
E.S. Kasischke, R.A. Shuchman, J.D. Lyden	135900-2-F_2
9. Performing Organization Name and Address	10. Work Unit No.
Environmental Research Institute of Michigan P.O. Box 8618 Ann Arbor, Michigan 48107	11. Contract or Grant No. DMA 800-78-C-0060
	13. Type of Report and Period Covered Final Report 9/25/79 - 4/30/80
12. Sponsoring Agency Name and Address	14. Sponsoring Agency Code
Defense Mapping Agency Hydrographic/Topographic Center Washington, D.C. 20315	

15. Supplementary Notes

The technical monitor for this report was Mr. James Hammack

16. Abstract

This report discusses a feasibility analysis of extracting bathymetric information from synthetic aperture radar (SAR) data collected by the SEASAT satellite. A SAR system can provide bathymetric information by recording variations in radar backscatter which are due to an interaction between a hydrographic feature and a physical oceanic process.

Data from four SEASAT passes were used to examine five study sites. These included two sites in the Bahamas, one site around Nantucket Island, one site in the English Channel and one site around North Rona Rock, Scotland.

Analysis techniques included bathymetric correlations (comparison of the position of SAR observed surface features to the position of distinct bottom topographic features), photographic enhancement and special optical processing techniques (to bring out additional, previously unobserved features on the SAR imagery), and relative radar backscatter measurements.

For the study sites chosen, a high degree of correlation existed between the SAR observed surface phenomena and bottom topographic features. At the two Bahama study sites, the SAR-observed surface features were quite subtle, and attempts to gain further information through photographic enhancement (cont)

17. Key Words	18. Distribution Statement
SEASAT Synthetic Aperture Radar Bathymetry Oceanography Radar Backscatter	

19. Security Classif. (of this report)	20. Security Classif. (of this page)	21. No. of Pages	22. Price
Unclassified	Unclassified	viii + 92	

16. (continued)

and optical processing techniques were not successful within the scope of this effort.

Relative radar backscatter measurements made at four of the five ~~study~~ sites indicated that a high percentage of the SAR observed surface features were positioned directly above a major bottom topographic feature. The backscatter measurements had variations as high as 6 dB.

[redacted]

PREFACE

The work described in this report was conducted jointly by the Radar and Optics Division and Applications Division of the Envrionmental Research Institute of Michigan. This work was supported by the Hydrographic/Topographic Center of the Defense Mapping Agency as part of Task 7 of Contract No. DMA-800-78-C-0060. The technical monitor was Mr. James Hammack.

The entire DMA contract was under the supervision of Mr. Fabian Polcyn, while Dr. Robert A. Shuchman was the Principle Investigator for Task 7. The purpose of Task 7 was to investigate the potential of using SEASAT synthetic aperture radar (SAR) data in providing bathymetric information. A companion volume to this report which discusses multispectral scanning techniques used to extract depth information is entitled "Evaluation of Water Depth Extraction Techniques Using Landsat and Aircraft Data" (Doak, et al., 1980).

Mr. Eric S. Kasischke performed the bathymetric correlations and the resulting analysis. Mr. James Lyden developed the computer programs to geometrically correct the digital SAR data and produced the bathymetric/radar cross sections figures. Mr. Alex Klooster produced the relative radar backscatter measurements on the ERIM optical processor/hybrid digitizer. Mr. James Marks produced the custom optically processed SAR imagery. Ms. Jacquelyn S. Ott made the SAR photo mosaics. The authors would like to thank Mr. James Hammack of DMA for providing the bathymetric charts used in this study, and Mr. Charles Reed of DMA for providing the Landsat data for the Nantucket Shoals area. The authors would also like to thank Mr. Walt Brown, Mr. Ben Holt and Ms. Elaine Xenos of the Jet Propulsion Laboratory for providing ERIM with SEASAT data for this study. The authors finally would like to thank Drs. M. Violler and N. Baussart of l'Univerite' des Sciences et Techniques de Lille, Villeneuve d'Ascq, France for the use of Figure 28 in this report.

CONTENTS

PREFACE	iii
LIST OF FIGURES	v
LIST OF TABLES	viii
1. INTRODUCTION	1
2. SUMMARY	3
3. BACKGROUND	5
3.1 SAR CONCEPTS	6
3.2 SEASAT SAR DATA	12
4. DATA SETS	15
5. BATHYMETRIC CORRELATIONS	19
6. PHOTOGRAPHIC ENHANCEMENT AND OPTICAL PROCESSING ANALYSIS	35
7. RELATIVE RADAR BACKSCATTER MEASUREMENTS	43
8. DISCUSSION	57
9. CONCLUSIONS AND RECOMMENDATIONS	71
REFERENCES	75
APPENDIX A: BATHYMETRIC CORRELATIONS	A-1
APPENDIX B: GEOMETRIC CORRECTION OF SEASAT SAR DATA	B-1

LIST OF FIGURES

FIGURE	TITLE	PAGE
1	SAR Imagery of Internal Waves Collected During SEASAT Revolution 1232, 21 September 1978	7
2	Schematic Diagram of Internal Wave Location from SEASAT Orbit 1232	8
3	SAR Imagery of Surface Anomalies Present During SEASAT Revolution 762, 19 August 1978, Between Scotland and Iceland	9
4	Diagram of Internal Waves Observed on SEASAT SAR Imagery from Orbit 762	10
5	Geographical Location of Study Areas	16
6	SAR Imaged Surface Features Near Nantucket Island (Study Site C) from SEASAT Revolution 880, 27 August 1978	20
7	Combination of Nantucket Island SAR Imagery (Revolution 880) and Bathymetric Chart	21
8	SAR Imaged Surface Feature Near Bimini Island (Study Site A) from SEASAT Revolution 407, 25 July 1978	24
9	SAR Imaged Surface Feature from Southern Edge of Great Bahama Bank from SEASAT Revolution 407, 25 July 1978	25
10	SAR Imaged Surface Features from the Thames River Estuary (Study Site D, Sub-Site 1) from SEASAT Revolution 762, 19 August 1978	28
11	Bathymetric Chart of Thames River Estuary	29
12	SAR Imaged Surface Features from the English Channel (Study Site D, Sub-site 2) from SEASAT Revolution 762, 19 August 1978	30
13	Bathymetric Chart of Northern English Channel	31
14	SAR Image Surface Feature near North Rona Rock, Scotland, from SEASAT Revolution 762, 19 August 1978	32

FIGURE	TITLE	PAGE
15	Combination of Figure 14 with Bathymetric Chart of North Rona Rock Area (depths in fathoms)	33
16	Variation of Radar Backscatter (σ_o) with Terrain Type and Grazing Angle	36
17	Examples of Photographic Paper Contrast for SEASAT Revolution 407 near Bimini Island	38
18	Examples of SAR Imagery Made Using Different Recording Film Types During Optical Processing (Rev. 651 Data)	40
19	Examples of SAR Imagery Made Using Different Azimuth Focus Corrections During Optical Processing (Rev. 651 Data)	42
20	Summary of Relative Backscatter Measurements Made at Study Site A (Bimini Island) from SEASAT Rev. 651, 19 August 1978	45
21	Summary of Relative Radar Backscatter Scans and Depth Transects Made at the Thames River Estuary Region, SEASAT Rev. 762, 19 August 1978	46
22	Summary of Relative Radar Backscatter Measurements and Depth Transects Made at the English Channel Region, SEASAT Rev. 762, 19 August 1978	47
23	Summary of Relative Radar Backscatter Measurements made at Study Site E (North Rona Rock) from SEASAT Rev. 762, 19 August 1978	48
24	SAR Imagery made from JPL Produced Digital Data, Nantucket Island, SEASAT Rev. 880, 27 August 1978	50
25	Location of Relative Radar Backscatter Measurement Transects for Rev. 880 Data	51
26	Relative Radar Backscatter Measurements and Depth Transects for Scan A, Nantucket Shoals, SEASAT Rev. 880, 27 August 1978	52
27	Relative Radar Backscatter Measurements and Depth Transects for Scan B, Nantucket Shoals, SEASAT Rev. 880, 27 August 1978	53
28	Relative Radar Backscatter Measurements and Depth Transects for Scan C, Nantucket Shoals, SEASAT Rev. 880, 27 August 1978	54

FIGURE	TITLE	PAGE
29	Schematic of the Structure of Progressive Internal Wave Motion Along a Sharp Thermocline Illustrating Alteration of Surface Roughness (after LaFond and Cox, 1962)	58
30	SEASAT Rev. 1411 over the Tongue of the Ocean (Bahamas)	62
31	Summary of Tidal Current Velocities at the Time of SEASAT Rev. 762 over the English Channel, 19 August 1978 (velocities are in knots, 1 knot = 1/2 meter/second)	63
32	Landsat Imagery of Study Site D, Sub-site 2 (English Channel)	64
33	Summary of Tidal Current Velocities and Wind Speed in the Nantucket Island Area at the Time of SEASAT Rev. 880, 27 August 1978 (velocities in knots, 1 knot = 1/2 meter/second)	66
34	Band 6 Landsat Imagery of the Cape Cod/Nantucket Island Area, Collected on 17 July 1974	68
B1	Transect Location, Rev. 880	B-3

LIST OF TABLES

TABLE	TITLE	PAGE
1	Summary of Data Types and Data Analysis Techniques	18
2	Summary of Bathymetric Correlations	22
A1	Bathymetric Correlations for Site A, DMA-Bahamas Photobathymetric Calibration Area, SEASAT Rev. 407	A-3
A2	Bathymetric Correlation for Site A, DMA-Bahamas Photobathymetric Calibration Area, SEASAT Rev. 651	A-4
A3	Bathymetric Correlation for Site C, Nantucket Shoals Area, SEASAT Rev. 880	A-5
A4	Bathymetric Correlation for Site D, Sub-site 1, Thames Estuary, SEASAT Rev. 762	A-9
A5	Bathymetric Correlation for Site D, Sub-site 2, English Channel, SEASAT Rev. 762	A-12

1
INTRODUCTION

The objective of this study was to evaluate the ability of synthetic aperture radar (SAR) data collected by the SEASAT satellite to provide information on bottom topography in oceanic areas. Investigations were undertaken to evaluate SEASAT's ability to detect uncharted or mispositioned submerged features hazardous to marine navigation, to position these features accurately, and to investigate whether or not depth information can be extracted from SAR data. Specifically, three analyses were performed. First, correlations were made between surface patterns present on SAR imagery in oceanic areas and hydrographic features. Secondly, techniques to enhance subtle SAR signatures indicative of bottom features were evaluated. And finally, several techniques to measure relative radar backscatter return were evaluated in an attempt to better quantify the relationship between the surface features and the related bottom topography.

The data studied in this report was collected by the SEASAT satellite. Among the instrumentation carried by SEASAT, which was launched during June of 1978, was a synthetic aperture radar (SAR). This satellite collected over 500 passes of SAR data before suffering a catastrophic power loss in October of 1978. The SAR on board SEASAT was an L-band (23.5 cm wavelength) radar. It collected 25 x 25 meter resolution imagery with a ground swath-width of 100 km and a length of up to 4000 km.

The wavelength at which the SEASAT SAR system operates (23.5 cm) does not penetrate more than a few centimeters into the water surface. Therefore, the recorded return signal is primarily reflected from the water's surface and is a function of the surface roughness and the surface slope. The surface features reported in this study are believed to be the result of a hydrodynamic interaction between a physical

oceanic process and a bottom topographic feature. This interaction results in an alteration of either the surface roughness or slope; hence a surface anomaly is observed on the SAR imagery.

Five different areas from four SEASAT orbits were studied. Initial comparisons between the surface features present in the coastal regions of these passes and bottom topography information were made to see if any correlation existed. In a very high percentage of the cases, a correlation did exist between a surface signature on the SAR imagery and a bottom topographic feature. During this analysis it was observed that in some areas the SAR surface signatures were distinct, while in other areas the surface features were quite subtle.

In those areas of subtle surface features, a second analysis was conducted to see if these subtle features could be made more visible through photographic enhancement and SAR-processing techniques. It was thought that these special processing techniques might also bring out features which were not previously visible on the survey processed (quick-look) imagery. The photographic techniques included photographic enlargements and use of different levels of contrast on the photographic paper. The SAR processing techniques involved special optical processing of the SAR signal film including motion corrections, looking at the proper dynamic range to display oceanographic applications, and variation of recording film types to test several film contrasts.

Relative radar backscatter measurements were made in the third analysis in an attempt to see if a quantitative relationship existed between the observed SAR radar returns and water depth. These relative backscatter measurements were obtained from the radar signal film using the ERIM hybrid digitizer and from JPL digitally processed data.

2

SUMMARY

This study evaluated the use of synthetic aperture radar (SAR) imagery collected by the SEASAT satellite to provide bathymetric information. The SAR system can provide bathymetric information by imaging surface perturbations which are a result from a hydrodynamic interaction between a physical oceanic process (such as a current or wave) and a distinct hydrographic feature.

Imagery from four SEASAT passes was used to study five study sites. These sites included: the DMA-Bahama Photobathymetric Calibration Area in the Northwestern Bahamas; a portion of the Southwestern Great Bahama Banks, just north of Cuba; the Nantucket Shoals region of Cape Code; portions of the English Channel; and the area surrounding North Rona Rock, off the coast of Scotland.

The surface features present in the two test sites in the Bahamas showed a high degree of correlation to bottom topographic features (60 to 100%), but were quite subtle, and were located only at the edges of the Great and Little Bahama Banks. Special photographic and optical processing techniques were used on these data to find other depth-related surface patterns but did not bring forth any additional information.

The surface patterns present in the other study sites were quite distinct and an examination of the position of these patterns revealed a strong correlation (77% or higher) relative to the position of distinct bottom topographic features, as obtained from bathymetric charts.

Relative radar backscatter measurements were obtained at four of the five test sites (the Southern Bahamas Test Site was excluded).

These backscatter measurements were produced in transect form and were compared to bathymetric cross-section transects of the same areas. A high percentage of the major bottom topographic features on the bathymetric cross-sections were positioned directly below a major surface feature on the SAR data (which is indicated by a significant [3-6 dB] drop or rise on the radar backscatter transect).

Also presented is ancillary information (such as tidal and meteorological data) and Landsat imagery which support the observation that the surface patterns present on the SAR imagery are an indirect result of a hydrodynamic interaction between a physical oceanic process (i.e., a current) and a distinct bottom topographic feature.

This study clearly demonstrates the feasibility of utilizing synthetic aperture radar imagery to provide bathymetric information. SAR can be used to detect the presence of certain types of bathymetric features and can provide a rough indication of their location. However, it should be noted, the limitations of SAR to obtain this information (i.e., under what oceanic and meteorological conditions) is not totally understood at present.

3
BACKGROUND

During examination of SEASAT Synthetic Aperture Radar (SAR) imagery, it was noted that a variety of surface anomalies existed, both in deep and shallow water areas. A theory has been postulated that many of these anomalies are a result of an interaction between a physical oceanic process and a distinct bottom feature, and as such, represent a way of using SAR imagery to gain bathymetric information.

Five different physical oceanographic phenomena have been observed on SAR imagery that permit detection of underwater hazards. These include:

1. The change in direction and wavelength of ocean swell as they enter coastal regions which can be observed on SAR imagery;
2. Observation of classic internal wave patterns over continental shelf regions;
3. Anomalous SAR backscatter signatures found in deep ocean regions over topographic "bumps" on the ocean bottom,
4. A distinct change in radar backscatter which is associated with an ocean swell propagating over a distinct depth discontinuity; and
5. A distinct change in radar backscatter which is associated with a current flowing over a bottom feature.

Models which incorporate the way an ocean waves changes as it enters shallow waters can be used to gain an estimate of water depths in coastal regions. When a gravity wave enters a shallow-water region from deep water, its wavelength and direction change in direct proportion to the water depth. By measuring the change in wavelength or direction, an estimate of the water depth can be obtained. Since a SAR can measure both ocean wavelength and direction, this information can be used in a wave refraction model. This was done in studies by Shuchman, et al. (1979).

Basic SAR/Oceanographic theory holds that the microwave energy from the radar is being reflected from the ocean's surface by the small capillary and ultra-gravity waves present at the ocean's surface. Capillary and ultra-gravity waves have wavelengths between one and fifty centimeters and are generated by winds. Any change in this small wave structure will alter the radar backscatter being received by the SAR.

Internal wave packets propagating shorewards over a continental shelf region act as a mechanism permitting SAR detection of changes in bottom form. The internal wave energy field alters the small capillary and ultra-gravity waves sufficiently so that the internal waves are visible on SAR imagery (Shuchman and Kasischke, 1979). An example of this phenomena is presented in Figures 1 and 2. Surface anomalies, similar to internal waves, but not as well structured (into wave packets), have been noticed on SAR images in deep-water areas between major continental shelf boundaries (Shuchman and Kasischke, 1979). The interesting fact about these surface anomalies is that in large part, they occurred over a major underwater ridge or seamount (see Figures 3 and 4).

DeLoor and VanHulten (1978) observed bottom-related surface features on radar imagery collected over shallow water regions of the North Sea.

3.1 SAR CONCEPTS

A SAR system offers several advantages over passive remote sensing techniques. Synthetic Aperture Radar is an active imaging device that senses the environment with short electromagnetic waves. As active sensors, radars provide their own illumination in the microwave region of the electromagnetic spectrum and thus are not affected by diurnal changes in emitted or reflected radiation from the earth's surface. Additionally, SAR's have the recognized advantage of being able to image the earth's surface independent of weather conditions or solar illumination and to provide synoptic views of the ocean at high resolution. Most radars operate in the frequency region of 300 MHz (1 m) to 30 GHz (1 cm), and bandwidths within this region are commonly designated by letters. The SEASAT SAR discussed in this paper is designated as an L-Band (23.5 cm) system.

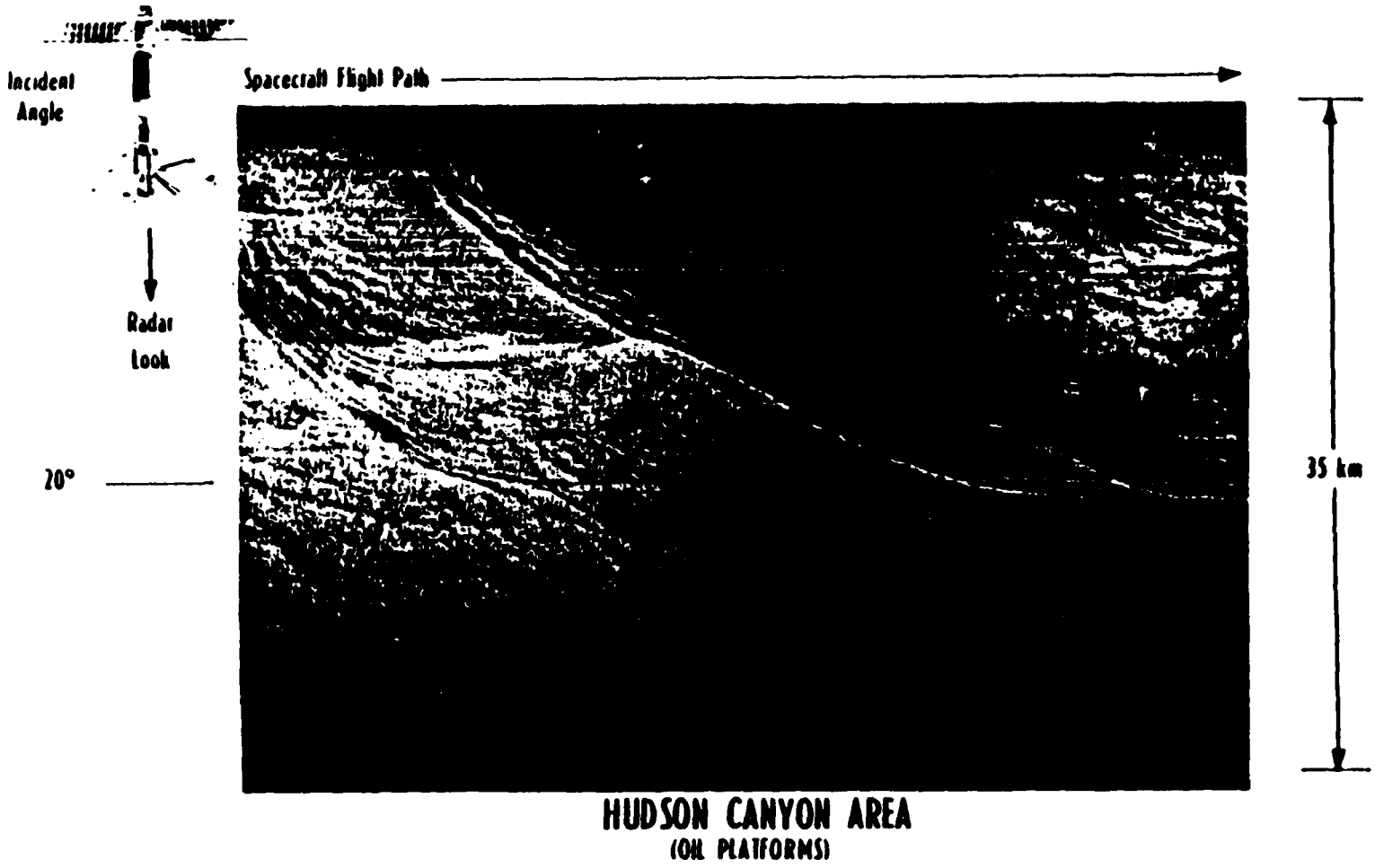

Figure 1. SAR Imagery of Internal Waves Collected During SEASAT Revolution 1232, 21 September 1978.

LONG ISLAND
Montauk Pt
NEW JERSEY
10fm
20fm
30fm
40fm
50fm
100fm
500fm
1000fm
Hudson Canyon
Area of SEASAT SAR
Imagery in Figure 1

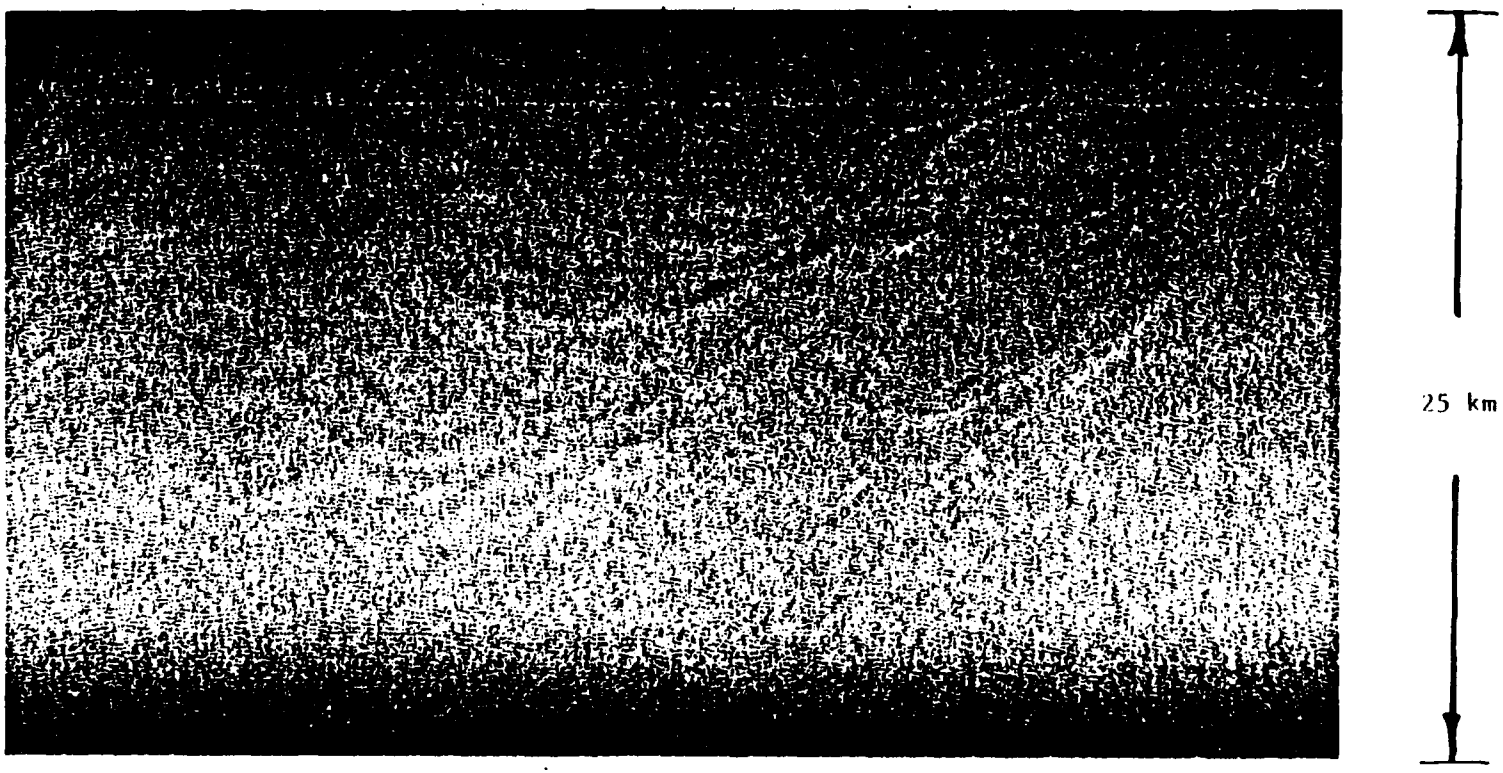

Figure 3. SAR Imagery of Surface Anomolies Present During SEASAT Revolution 762, 19 August 1978, Between Scotland and Iceland.

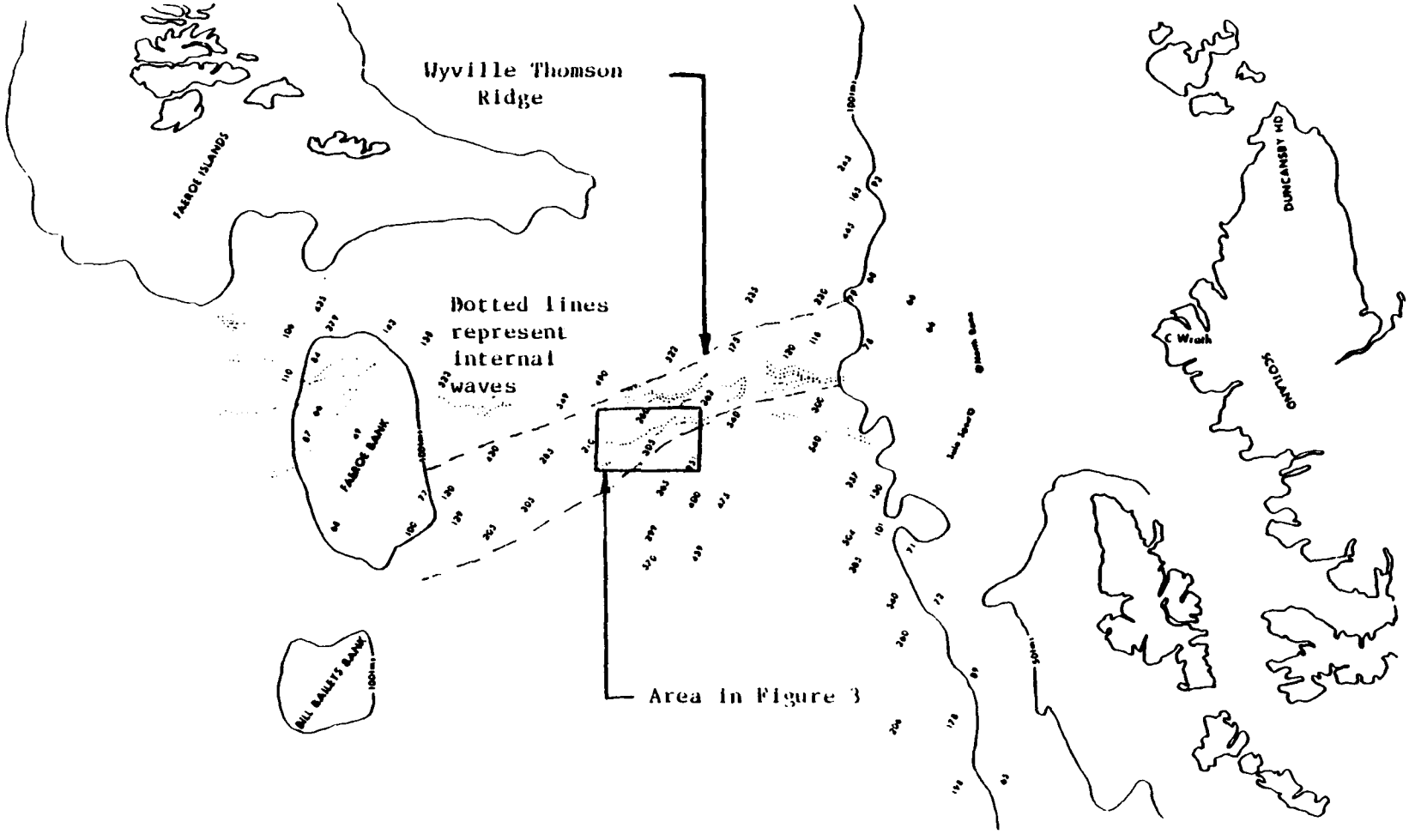

FIGURE 4. DIAGRAM OF INTERNAL WAVES OBSERVED ON SEASAT SAR IMAGERY FROM ORBIT 762.

Synthetic Aperture Radar is a coherent airborne or spaceborne radar that uses the motion of a moderately broad physical antenna beam to synthesize a very narrow beam thus providing fine azimuthal (along-track) resolution (Brown and Porcello, 1969; Harger, 1970). Fine range (cross-track) resolution is achieved by transmitting either very short pulses or longer coded pulses which are compressed by matched-filtering techniques into equivalent short pulses. Usually, the coded pulse is a waveform linearly modulated in frequency.

Typically, the phase history of a scattering point in the scene is recorded on photographic film as an anamorphic (astigmatic) Fresnel zone plate. The parameters of the zone plate are set in the azimuth direction by the Doppler frequencies produced by the relative motion between the sensor and the point scatterer, and in the range direction by the structure of the transmitted pulses. The film image is a collection of superimposed zone plates representing the collection of point scatterers in the scene. This film is used by a coherent optical processor which focuses the anamorphic zone plates into the points which produced the microwave scatter of the scene (Kozma, et al., 1972). Recently, SAR processing has employed digital techniques.

However, when using a SAR system to image moving targets such as the ocean surface, unique problems occur when correlating the signal data. Because moving targets (such as waves or currents) perturb the Doppler frequencies, and hence the phase histories recorded by the signal receiver, conventional processing of these signal histories produces images of the ocean that are defocused relative to a stationary target. Defocusing by the along-track (azimuth) velocity of moving ocean surfaces can be refocused by re-adjusting the azimuth focus (cylindrical focus) an amount proportional to the relative velocity of the ocean surface.

Similarly, the radial motion of a moving ocean surface imaged by a SAR will also perturb the signal history of a scatterer. Radial velocity (motion towards the radar look direction) produces an apparent tilt to the phase history as recorded by the signal receiver. Additionally, the scatterer history will also shift across the signal record. This is referred to as "range walk" and can be compensated for by a rotation of the cylindrical optics in the processing of the signal histories.

The signal histories recorded by a SAR frequently have a range of return brightness spanning 60 decibels (dB). This range of signal returns exists whether the histories are recorded in a digital or optical format (on SAR signal film). Problems arise when converting the signal histories to ouptut images in either an optical or digital format.

If the output product desired is an image film, it must be realized that most photographic emulsions can only record light intensities with a dynamic range of 17-20 dB with a linear response. Further, because of brightness compressions associated with this non-linear response pattern, many small reflectivity variations in an image can be lost due to "lumping" of brightness levels at the extreme ends of the intensity response window. Thus a film representation of SAR output imagery can "mash" features detected by the SAR.

The large dynamic range scenes imaged by a SAR can be displayed on film by creating a number of output films encompassing the entire dynamic range of a scene imaged by SAR (Larson, et al., 1975). If computer compatible tapes (CCT's) are used to store SAR output then approximately 40 dB worth of information can be retained.

3.2 SEASAT SAR DATA

Before entering into a discussion of the various measurement and analysis techniques used during this project, we should first mention the various forms the SEASAT SAR data are available to the user. SEASAT SAR data can be obtained in three ways: 1) JPL survey processed imagery; 2) SAR Doppler signal histories: and, 3) digital imagery and tapes.

JPL survey processed data is available to the user in either a master positive or a master negative form. Each pass of SEASAT data covers four sections of 70 mm wide film, with each section containing a 25 kilometer swath of data. The scale factor of this imagery is approximately 1:500,000 with a resolution of 30-40 meters. This data is relatively inexpensive and can usually be obtained in a few weeks. This data has been nominally geometrically corrected and usually is adequate for a quick first-look. The disadvantages associated with this data type are: 1) the imagery is a third generation film product; 2) the data is not always optimally processed with respect to the proper dynamic range for oceanographic observations and the full dynamic range of the data is unexploited; 3) a limited number of the total SEASAT passes are available in this form; 4) the imagery has not been processed to account for ocean surface motion; and, 5) the full potential resolution of the SAR system is not realized.

The second type of SEASAT SAR data utilized in this study was the SAR Doppler signal histories recorded on film. The difference between signal film and image film should be noted at this time to avoid confusion. Signal film is used to record the phase history of the various scattering points on the ground being illuminated by the SAR. By passing a collimated beam of monochromatic light through this signal film within an optical processing system, the ground image is reconstructed. By placing a recording film in the output plane, an image film is created.

The advantages of using SAR signal film lies in the fact that one can custom process the data according to the needs of the analyst. The data can be geometrically rectified, the proper dynamic range of the data for oceanographic applications can be used, maximum resolution

can be obtained (10 meters), and any image films are first generation film products. In addition, other output products are available. Digitized data (on CCT's) can be obtained and relative radar backscatter measurements can be made by placing a recording densitometer in the output plane of the optical processor. The main disadvantages of this data source are that special sophisticated processing facilities are needed, and associated with these facilities are considerable manpower expenses.

The last source of SEASAT SAR data available are digitally processed computer compatible tapes. These tapes are typically available from the Jet Propulsion Laboratory (JPL). Each JPL CCT contains a single 100 x 100 kilometer scene and the 25 meter resolution data has not been geometrically rectified. The advantages of this data source is that close to the full (up to 37 dB) dynamic range of the data can be exploited, very high quality photo imagery can be produced, and a variety of computer based analyses can be performed. The JPL CCT's disadvantages are: 1) the data has not been geometrically rectified; 2) the scene sizes are only 100 x 100 kilometers, with a limited number of scenes available; 3) the amount of information (36 million bytes) in each scene requires a large computer, and because of this large size, processing is quite expensive; and, 4) processing of this data requires a set of sophisticated software programs.

4
DATA SETS

The choice of test sites was a compromise between 1) selecting enough data sets to adequately sample the variety of conditions which produced (apparent) bottom related surface signatures; 2) the availability of SEASAT SAR data in coastal regions; 3) the different techniques available to analyze the data, and the different data products available of the test sites; and, 4) the availability of resources to adequately analyze the data as outlined in the statement of work.

Accordingly, five test sites were chosen (see Figure 5):

Site A: DMA-Bahamas Photobathymetric Calibration Area. The area in and around Bimini Island (the northwestern corner of the Great Bahama Bank) and the area in and around the western tip of Grand Bahama Island (the southwestern corner of the Little Bahama Bank).

Site B: Southern Bahamas. The southwestern corner of the Great Bahama Banks.

Site C: Nantucket Island. The shoal area immediately east of Nantucket Island, Massachusetts, including the Nantucket Shoals and the area just southeast of Cape Cod.

Site D: English Channel. The northern area of the Straits of Dover and the Thames Estuary region.

Site E: North Rona Rock. An area northwest of Cape Wrath, Scotland, surrounding the island referred to as North Rona Rock.

Data from four different SEASAT orbits were used for the various analyses. Study Sites A and B were covered by two different SEASAT orbits: Revolution 407, an ascending orbit, passed over the two test

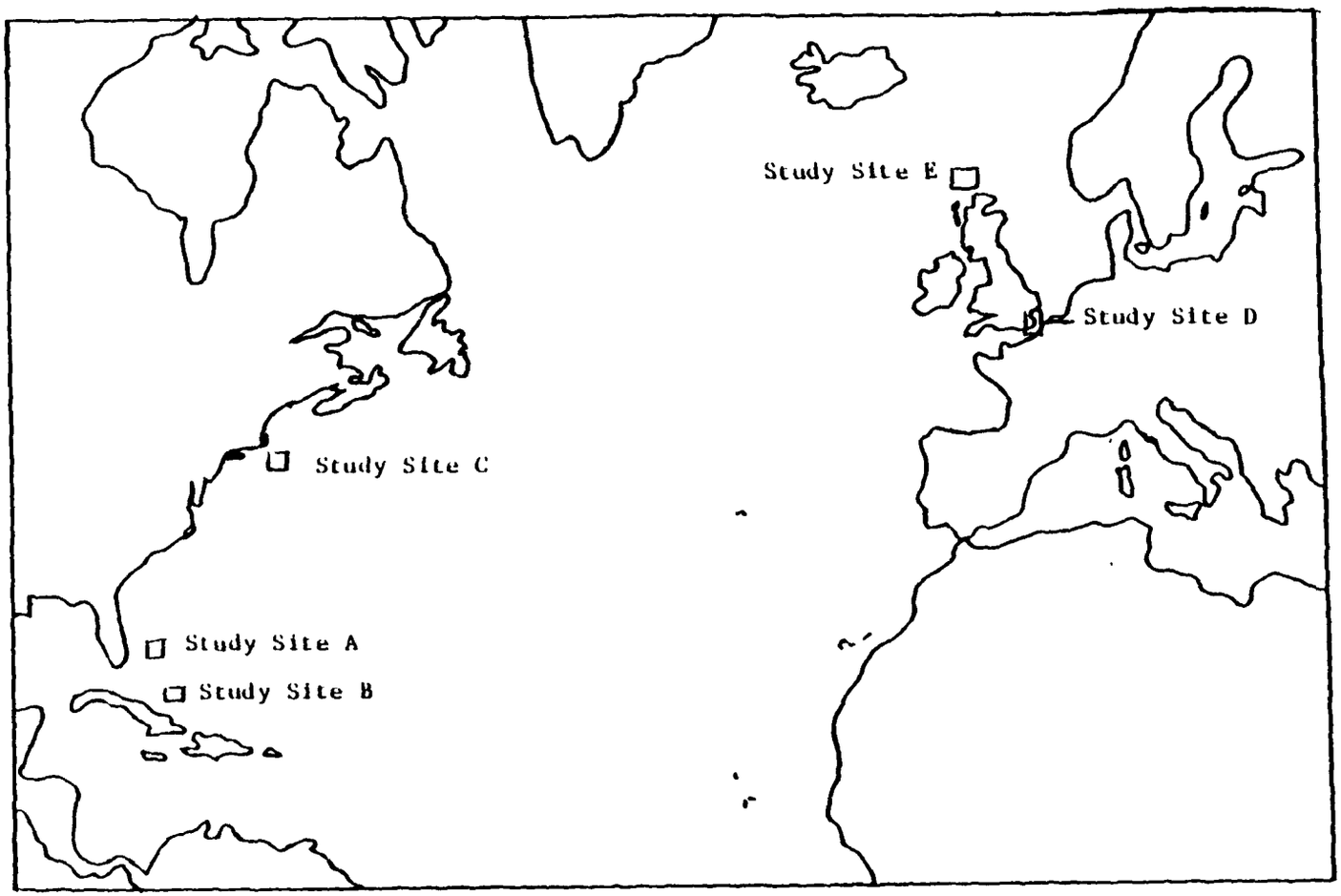

FIGURE 5. GEOGRAPHICAL LOCATION OF STUDY AREAS.

sites at approximately 12:46 (GMT) on 25 July 1978; and Revolution 651 was collected on 11 August 1978 at approximately 12:26 (GMT). Study Site C was covered during SEASAT Revolution 880 (an ascending pass) on 27 August 1978 at 12:34 (GMT). Finally, data for Study Sites D and E were collected during SEASAT Revolution 762 (an ascending pass) on 19 August 1978 at 6:47 (GMT).

Table 1 gives a summary of the Study Sites, the SEASAT Revolution(s) used for each Site, the data types available (for this study) for each SEASAT Revolution, and a summary of the analysis techniques used.

TABLE 1. SUMMARY OF DATA TYPES AND DATA ANALYSIS TECHNIQUES

STUDY SITE	SEASAT REVOLUTION	DATA TYPES	ANALYSIS TECHNIQUES
Site-A DMA-Bahamas Photobathymetric Calibration Area	407	JPL Survey	1. Bathymetric Correlation 2. Photographic Enhancement (and re-evaluation of bathymetric correlations)
	651	JPL Survey	1. Bathymetric Correlation
		Signal Film	1. Bathymetric Correlation (from image film) 2. Special Optical Processing (and re-evaluation of bathymetric correlations) a. Photo Enhancement b. Motion Correction 3. Hybrid Digitizer Backscatter Measurements
Site B - Southern Bahamas	407	JPL Survey	1. Bathymetric Correlation
	651	JPL Survey	1. Bathymetric Correlation
Site C - Nantucket Island	880	JPL Survey	1. Bathymetric Correlation
		JPL Digital	1. Backscatter Measurements
Site D - English Channel	762	Signal Film	1. Bathymetric Correlation (from image film) 2. Hybrid Digitizer Backscatter Measurements
Site E - North Rona Rock	762	Signal Film	1. Bathymetric Correlation (from image film) 2. Hybrid Digitizer Backscatter Measurements

5
BATHYMETRIC CORRELATIONS

The first analysis performed on each SAR data set was to overlay a clear transparency reproduction of a hydrographic chart onto the SAR imagery to see how closely the surface signatures correlated to bathymetric features (this process will be referred to as bathymetric correlation). The purpose of these bathymetric correlations was to see if the observed features occurred near a distinct bottom feature. What was looked for in this analysis were general correlations. If a surface feature occurred near (i.e., within a few hundred meters), but not exactly above a bottom topographic feature, a correlation was said to exist.

Figure 6 shows a photo mosaic made from the four sub-swaths of the JPL produced imagery of SEASAT Revolution 880, over Study Site C. Figure 7 is a blow-up of the area around Nantucket Island with a hydrographic chart overlay. These figures serve to illustrate both the type of SAR imaged oceanic surface features being studied, and the degree of correlation which existed between these features and bottom topographic information.

Table 2 summarizes the bathymetric correlations. Given in Table 2 are the Study Site, SEASAT Revolution used and percent correlation. Percent correlation was obtained for a given Study Site and Revolution by comparing the positions of the surface features on the SAR imagery to the position of distinct bottom topographic features from bathymetric charts and determining the ratio of the SAR features which occurred over a bathymetric feature. For example, at Study Site C (Nantucket Shoals), the 77 percent correlation figure was obtained by observing that 36 out of the 47 distinct surface patterns noted on the SAR

Figure 6. SAR Imaged Surface Features Near Nantucket Island (Study Site C) From SEASAT Revolution 880, 27 August 1978.

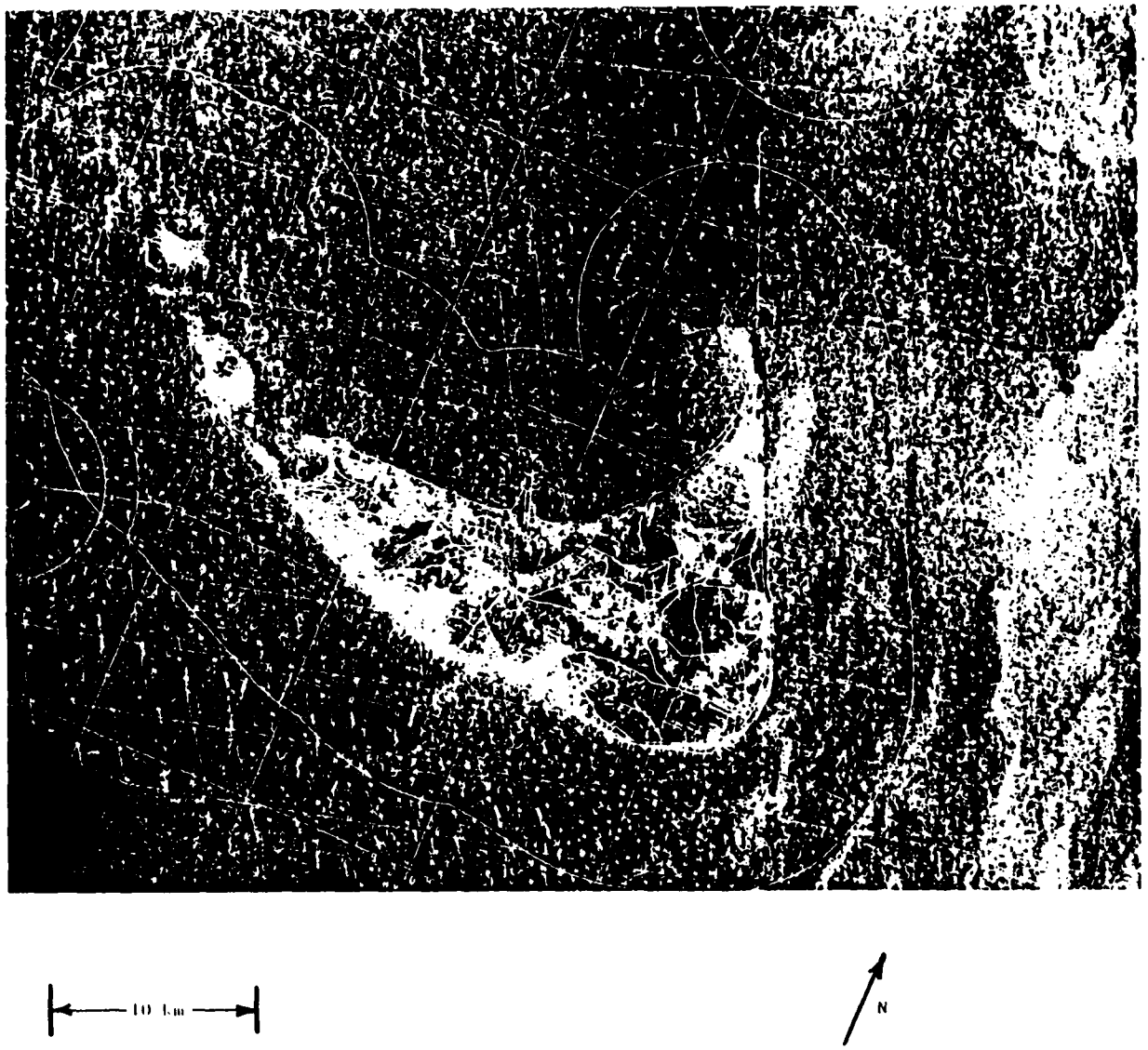

Figure 7. Combination of Nantucket Island SAR Imagery (Revolution 880) and Bathymetric Chart.

TABLE 2. SUMMARY OF BATHYMETRIC CORRELATIONS

STUDY SITE	SEASAT REVOLUTION	PERCENT CORRELATION
A - DMA-Bahamas Photo-bathymetric Calibration Area	407	60
	651	80
B - Southern Bahamas	407	100
	651	100
C - Nantucket Shoals	880	77
D - English Channel	762	
Sub-Site 1: Thames River Estuary		93
Sub-Site 2: English Channel		100
E - North Rona Rock	762	100

imagery (see Appendix A) occurred over a distinct bottom topographic feature. A complete discussion of this procedure and a summary of the individual data sets are presented in Appendix A.

The next portion of this section will present a brief written summary of bathymetric correlations along with some examples of the SAR image features.

The bottom-related surface features at Study Site A were along the edges of the Great Bahama Bank (near Bimini Island) and the Little Bahama Bank (near Grand Bahama Island). Figure 8 shows an example of a surface feature (near Bimini Island)which were typical of this area. No bottom-related surface features were noted on either Bahama Banks except near the Isaac Island group on Revolution 651 imagery, and near Bimini Island. The shallow, tidal flat area on the southeast side of Bimini was evident on the SAR imagery, as were the line of scattered rocks and islets just south of Bimini.

The surface features noted on SAR imagery from Site B (Southern Bahama, see Figure 9) were quite similar to those from Site A. Again, surface features were present near the edge of the Great Bahama Bank, just north of Cuba, on both passes of SEASAT imagery over this area. It should be noted that the bottom-related surface features in Study Sites A and B were quite subtle, which led to the second analysis, an attempt to enhance these subtle features through photographic and optical processing techniques. This analysis will be presented in the next section.

Almost 80% of the surface features present on the imagery from Site C (Nantucket Shoals) were over or near a distinct bottom feature (see Figures 6 and 7). This correlation improves to 94% when only those features in water less than 20 meters in depth were considered.

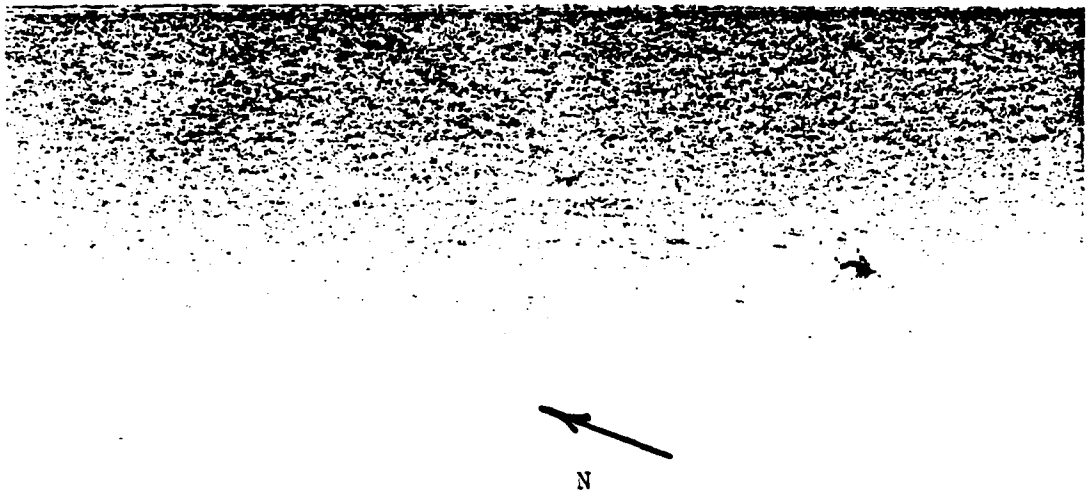

Figure 8. SAR Imaged Surface Feature Near Bimini Island (Study Site A) From SEASAT Revolution 407, 25 July 1978.

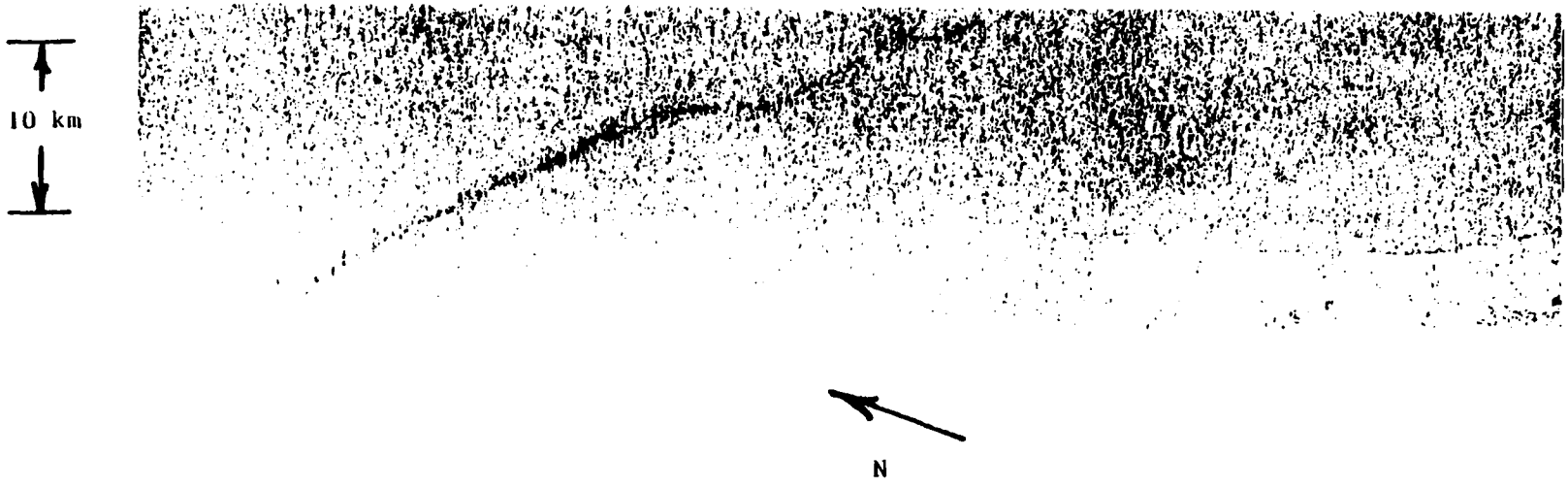

Figure 9. SAR Imaged Surface Feature From Southern Edge of Great Bahama Bank From SEASAT Revolution 407, 25 July 1978.

Study Site D was divided into two sub-sites for analysis. Sub-site 1 (see Figures 10 and 11) consists of an area in the Thames River Estuary slightly northwest of Ramsgate, England. Sub-site 2, a deeper water area, is a portion of the English Channel northwest of Dunkirk, France (see Figures 12 and 13). In sub-site 1, where a 93% correlation was found, numerous sand and mud banks are present, and the surface features occurred over or near these. In sub-site 2, where a 100% correlation was found, the features were present over a series of linear-shaped shoals in the middle of the English Channel.

Figure 14 shows SAR imagery from over Study Site E, North Rona Rock. Here, the oval-shaped surface feature corresponds to a shoal area which surrounds this island, as can be seen in Figure 15.

Figure 10. SAR Imaged Surface Features From the Thames River Estuary (Study Site D, Sub-Site 1) From SEASAT Revolution 762, 19 August 1978.

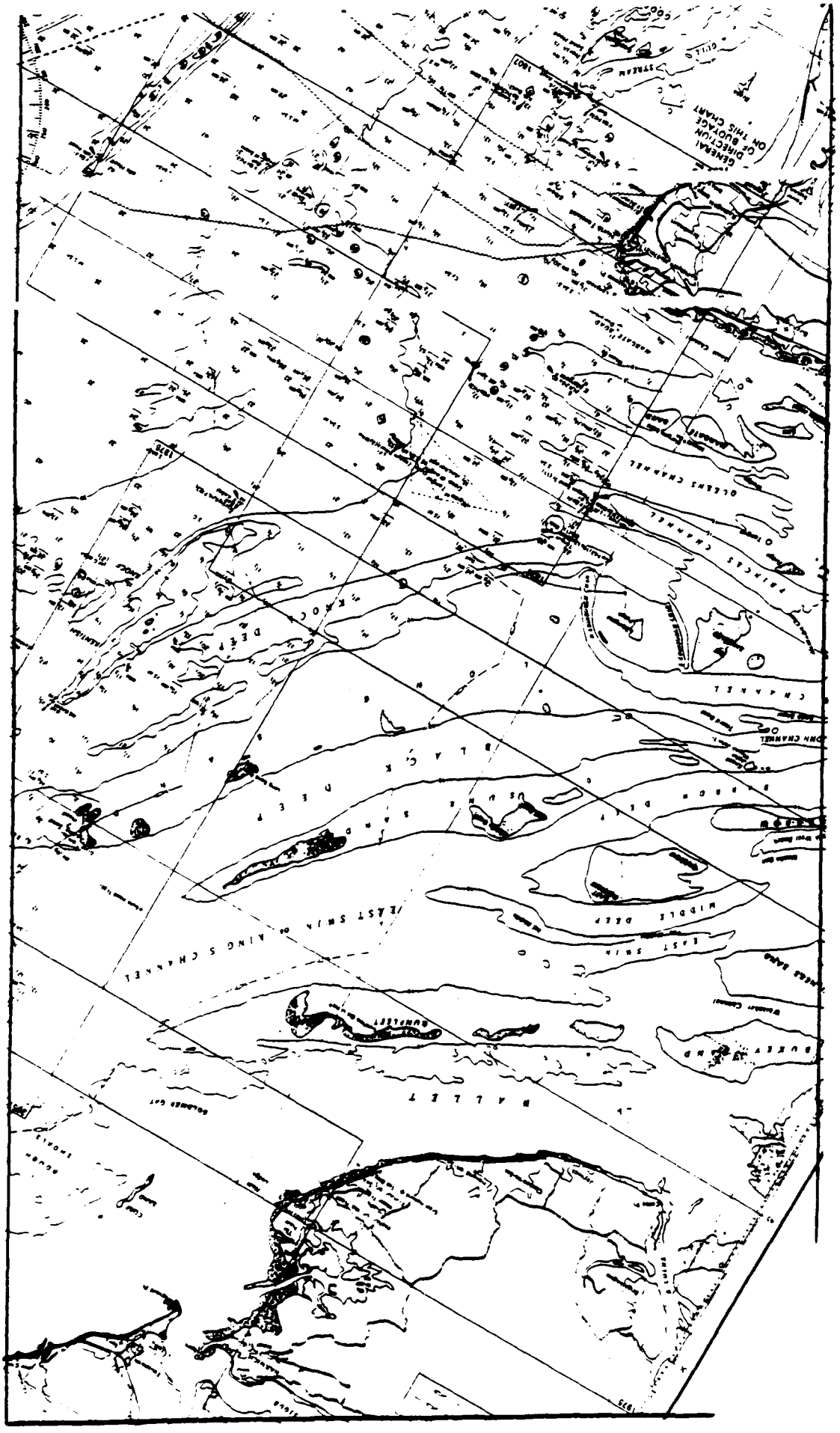

Figure 11. Bathymetric Chart of Thames River Estuary (see Figure 10 for corresponding SAR imagery).

Figure 12. SAR Imaged Surface Features from the English Channel (Study Site D, Subsite 2) from SEASAT Revolution 762, 19 August 1978

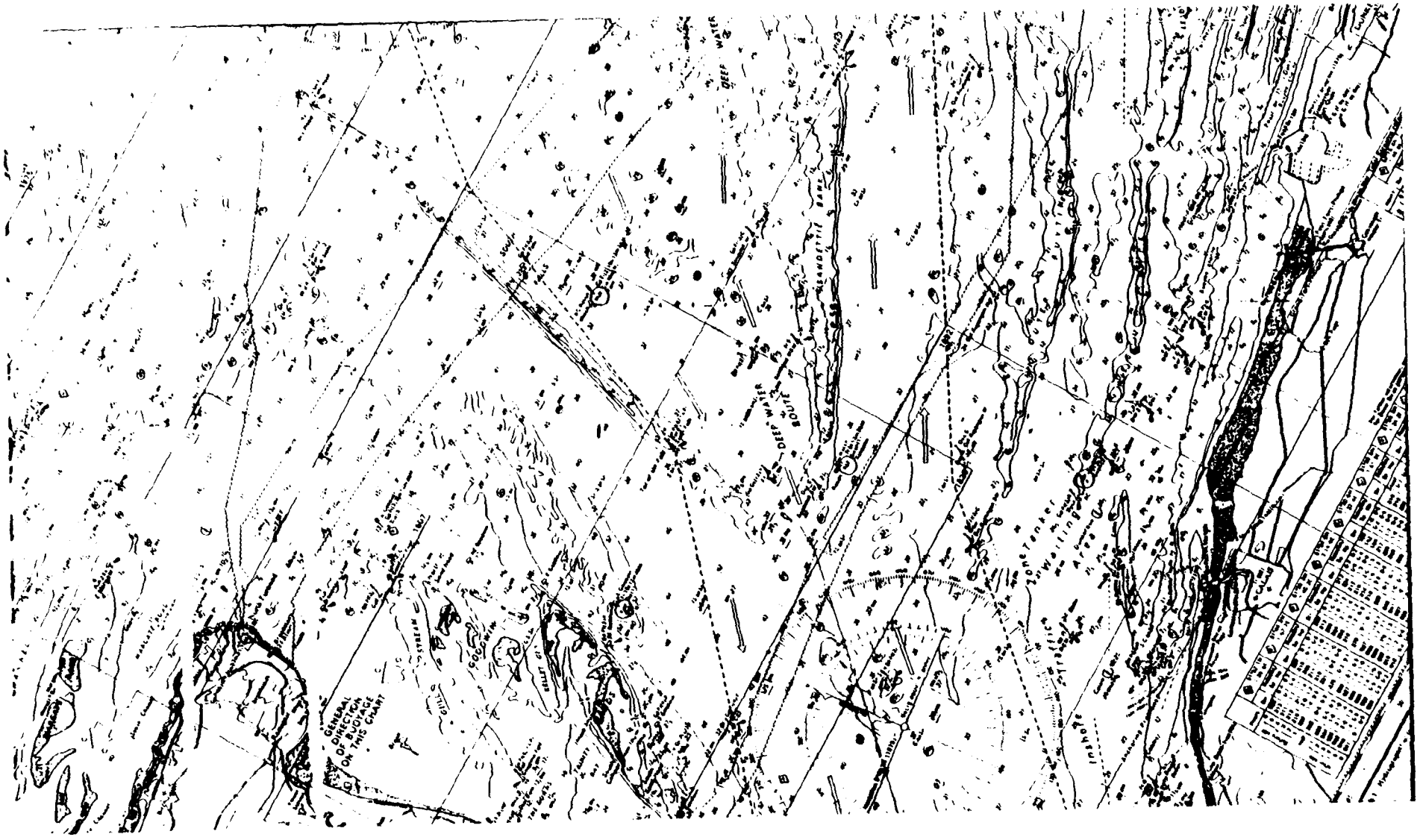

Figure 13. Bathymetric Chart of Northern English Channel (see Figure 12for corresponding SAR imagery).

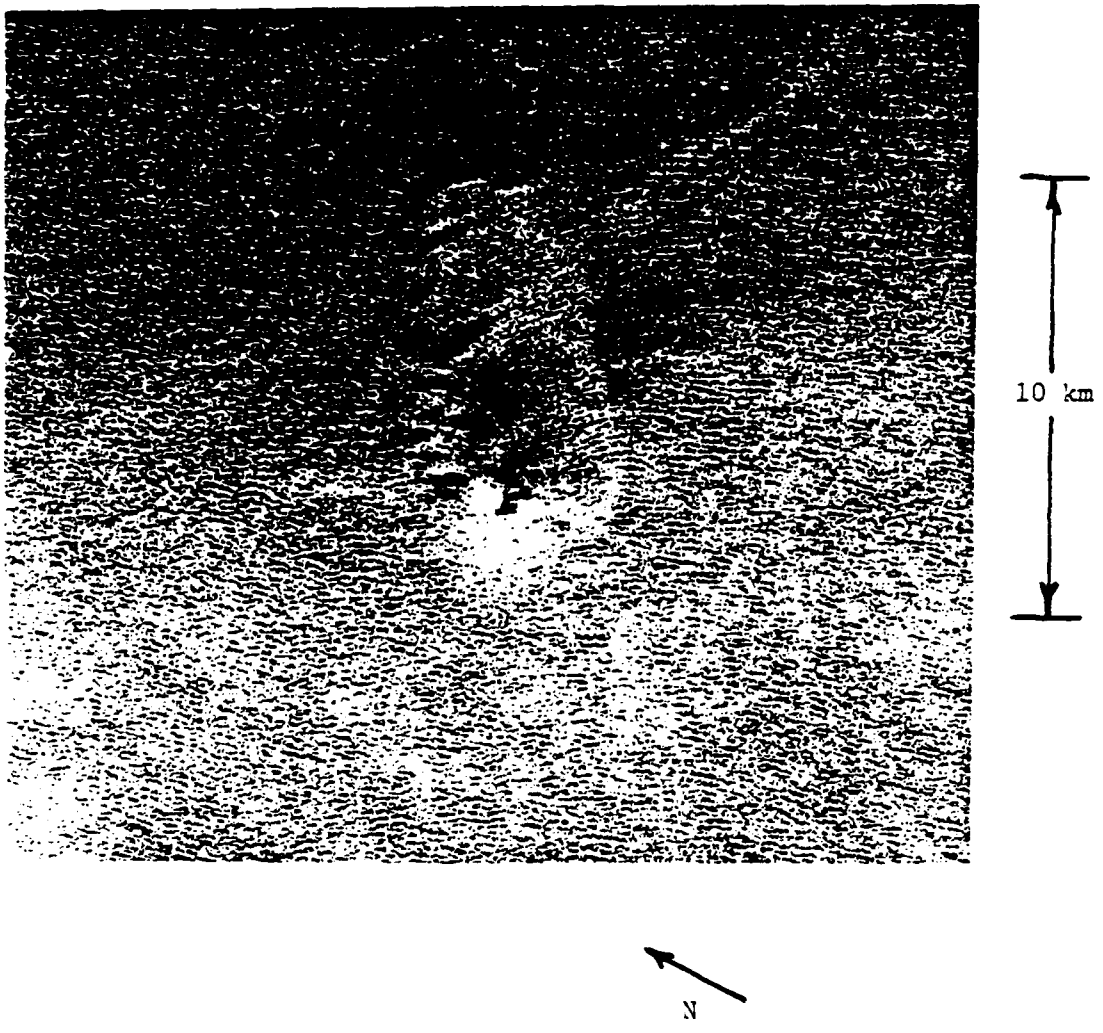

Figure 14. SAR Image Surface Feature near North Rona Rock, Scotland, from SEASAT Rev. 762, 19 August 1978

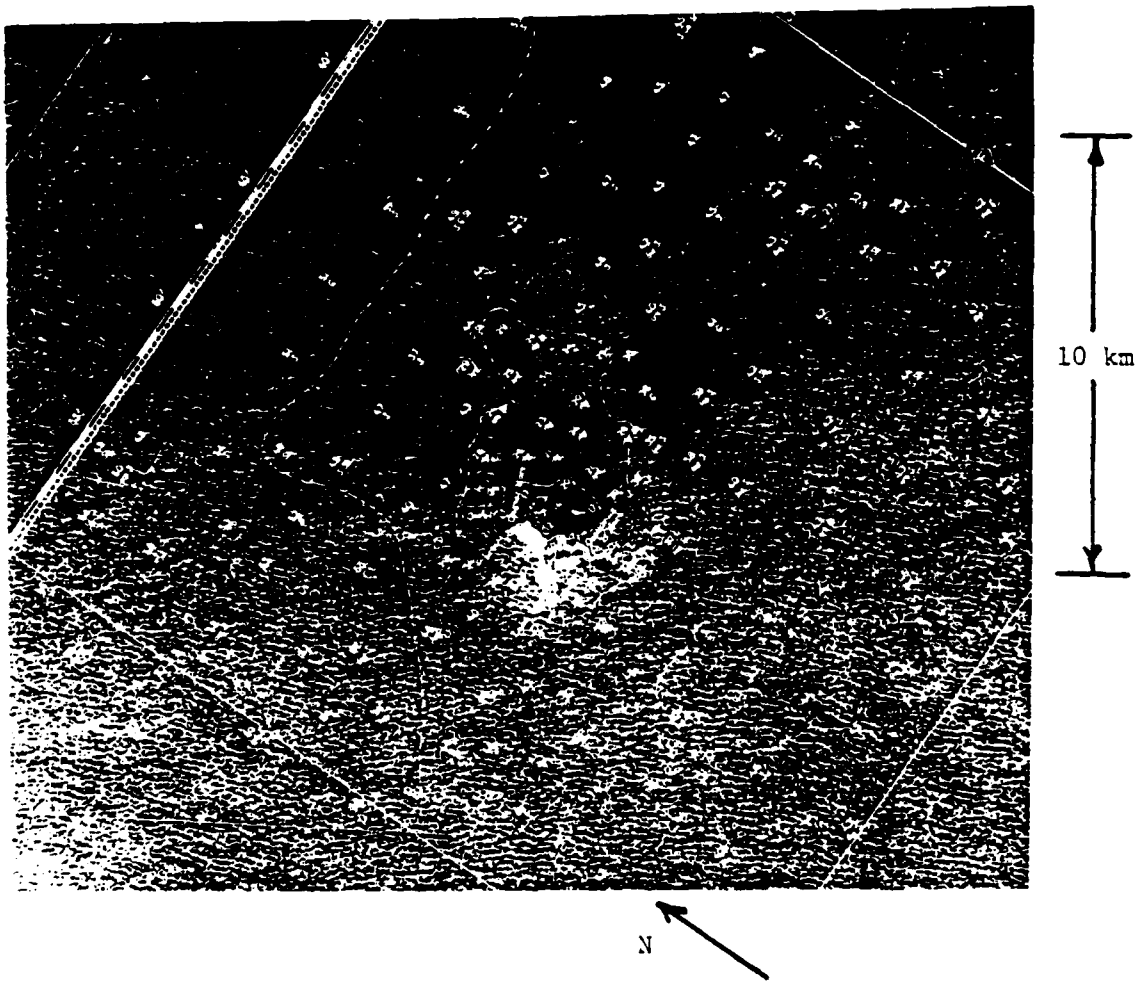

Figure 15. Combination of Figure 14 with Bathymetric Chart of North Rona Rock Area (depths in fathoms).

6
PHOTOGRAPHIC ENHANCEMENT AND OPTICAL PROCESSING ANALYSIS

As mentioned in the previous section, some of the bottom-related surface signatures observed on the SEASAT imagery were quite subtle in nature, while others were quite distinct. Study Sites A and B fell into the first category, and Sites C, D, and E, the latter. Because much previous work has been conducted at Study Site A (DMA-Bahamas Photobathymetric Calibration Area) in the field of remote sensing bathymetry, excellent ground truth exists for this area. Therefore, the decision was made to both photographically enhance and conduct special optical processing of the SEASAT SAR data from this area. The purpose of these special techniques was to see if additional bottom-related surface signatures could be seen on the imagery, as well as make any present (but subtle) features more distinct.

There are several reasons for attempting special techniques in processing SEASAT SAR data. The first concerns exploiting the proper dynamic range window for oceanographic applications. Radar backscatter (σ_o) is the way in which the radar return signals are discussed. These backscatter measurements are commonly converted to decibel (dB) values. Radar backscatter signals have a dynamic range covering up to 60 dB (see Figure 16). The radar signal film is processed onto output (image) film, which has a dynamic range of only 17-20 dB. One can either compress the data or only exploit a certain part of the data, depending on the application, when recording the data on output film. Radar signals have to be compressed before putting them on film.
One can assign a certain wide band (i.e., dB range) of data to a narrower band, thus enabling the recording of essentially the entire band (or dB) width onto the recording medium. In either case, information is lost. With JPL survey processed data, one does not know what part of the entire dynamic range of the SEASAT data has been displayed or what sort of data compression has been used. Custom optical processing of SAR signal film allows exploitation of the proper dynamic range for oceanographic studies.

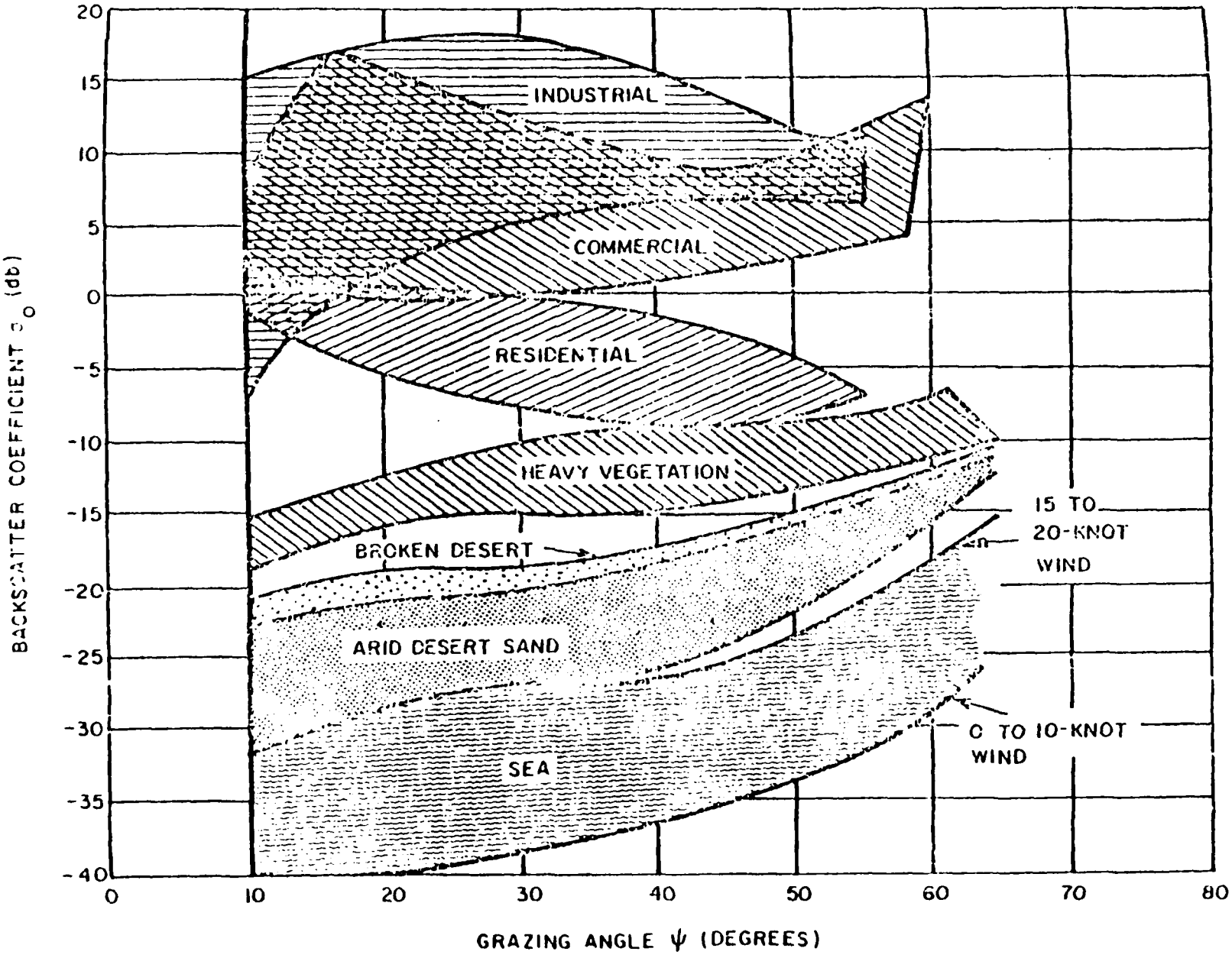

Figure 16. Variation of Radar Backscatter (σ_0) with Terrain Type and Grazing Angle

Surface features which are present on SAR imagery over ocean areas are most likely due to a physical oceanic process. The term "physical oceanic process" implies a motion-related process. Previous SAR studies (see Shuchman and Zelenka, 1978 and Teleki, et al., 1978) have indicated that the SAR ocean surface imaging mechanism is sensitive to motion effects of the radar backscatterers. Under certain circumstances these motion-related distortions can be corrected when processing the SAR signal histories and additional surface features become visible. No such corrections were made when the JPL survey processed imagery was produced.

JPL survey processed film from SEASAT Revolution 407 underwent special photographic processing in an attempt to enhance those features present and bring out previously undetected signatures. First, photographic prints were made using low and high contrast photographic paper. An example of low, normal and high contrast images from the area around Bimini Island are presented in Figure 17. Next, three to four times enlargements were produced and examined for possible bottom-related features. Upon examination of these sets of images, it was concluded that both these techniques provided little or no more information than the survey processed imagery. This result was not entirely unexpected. The general shape of the bottom in this area resembles a flat or gently rolling feature. Therefore, any water flow over this bottom type would generally be less turbulent than say over distinct shoals (such as around Nantucket Island).

Next, SAR signal film from SEASAT Revolution 651 underwent special optical processing. Three analyses were run: 1) adjustments were made so the optimum dynamic range for oceanographic applications was displayed on the output film; 2) different recording films with different Gammas (contrasts) were used; and 3) azimuth focus corrections were used to compensate for moving ocean surfaces imaged by the SAR.

One test was run where the optimum range was exploited while testing various film types which differed as to their Gammas. (Gamma is a

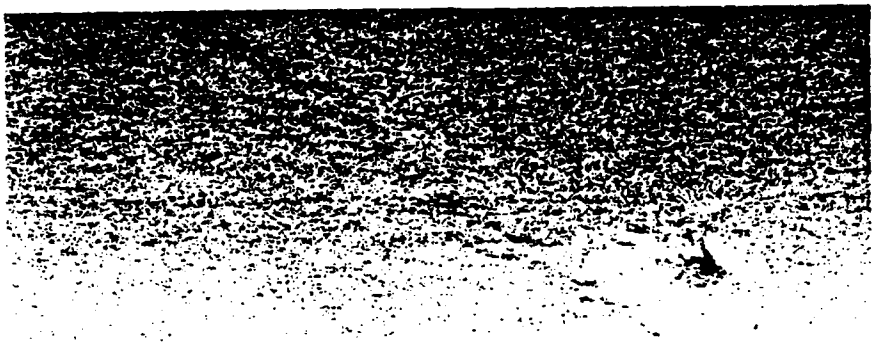

a. High contrast

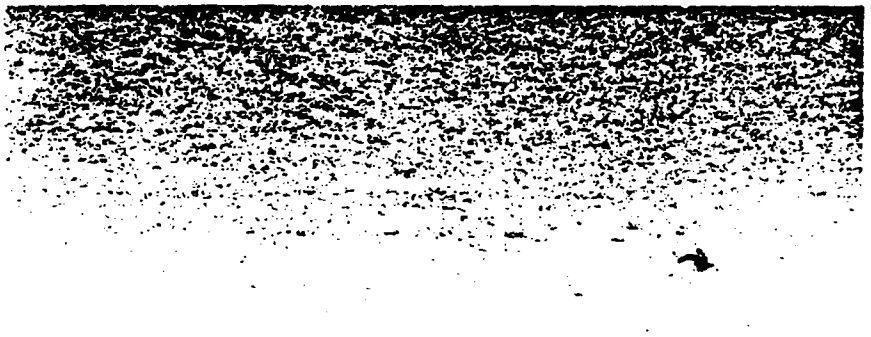

b. Normal contrast

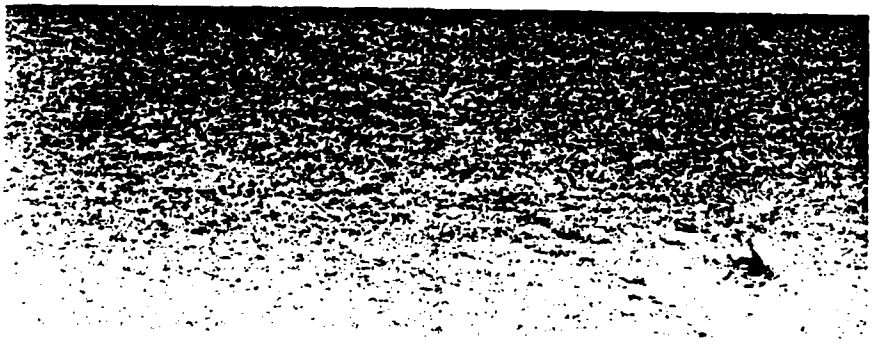

c. Low contrast

Figure 17. Examples of Photographic Paper Contrast for SEASAT Rev. 407 near Bimini Island

measure of the contrast of the film, the higher the Gamma, the greater the contrast). By processing Kodak EK3414 film on an automatic Versamat Machine, the highest Gamma of 1.7 was obtained. By processing Kodak panchromatic on the Versamat, a Gamma of 0.8 was obtained. By hand processing the EK3414 film, a low Gamma of 0.6 was obtained.

Figure 18 gives an example of each of the different Gammas used. Upon examination of these films, it was again observed that no additional surface anomalies could be detected.

A study to see if an azimuth focus correction results in enhanced imagery was conducted next. The Depth of Focus (D.F.) for this imagery (see Shuchman and Zelenka, 1978) is:

$$D.F. = \frac{2}{\lambda_\ell} \left(\frac{V_f}{V_{SAT}} \frac{\rho_a}{M}\right)^2 \qquad (1)$$

where: λ_ℓ (Illumination wavelength) = 0.6328×10^{-6} meters,

$\frac{V_f}{V_{SAT}} = \frac{1}{207,000}$, where V_f is the speed of the signal film, and V_{SAT} is the velocity of the SEASAT satellite),

ρ_a (Azimuth Resolution) = 10 meters

M (Processor Azimuth Demagnification) = 3.5

A depth of focus of 0.6 mm or 2.4×10^{-3} inches was calculated for the data. Based on this value, a series of images was made where the azimuth focus shift was changed in steps of approximately 2 x D.F. (5.0×10^{-3} inches). A series of output films were made using 6 different focus settings +4 D.F. (+.01 inches), +2 D.F. (+.005 inches),

10 km

a) Gamma of 1.8 (high contrast)

N

b) Gamma of 0.8

c) Gamma of 0.6 (low contrast)

Figure 18. Examples of SAR Imagery Made Using Different Recording Film Types During Optical Processing (Rev. 651 Data)

0 D.F. (0.00 inches), -2 D.F. (-0.005 inches), -4 D.F. (-0.01 inches), and -6 D.F. (0.015 inches). Several of these variable focus setting films are illustrated in Figure 19. Again, no additional surface features were detected on the specially focused data.

10 km

a) + 4 Depths of Focus

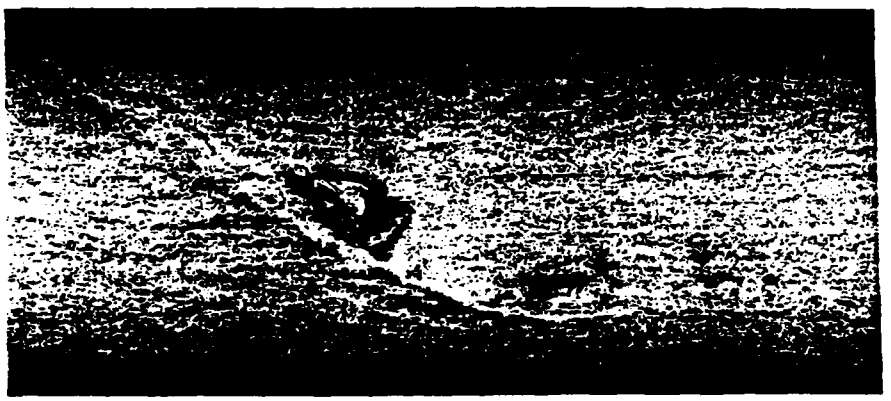

N

b) 0 Depths of Focus

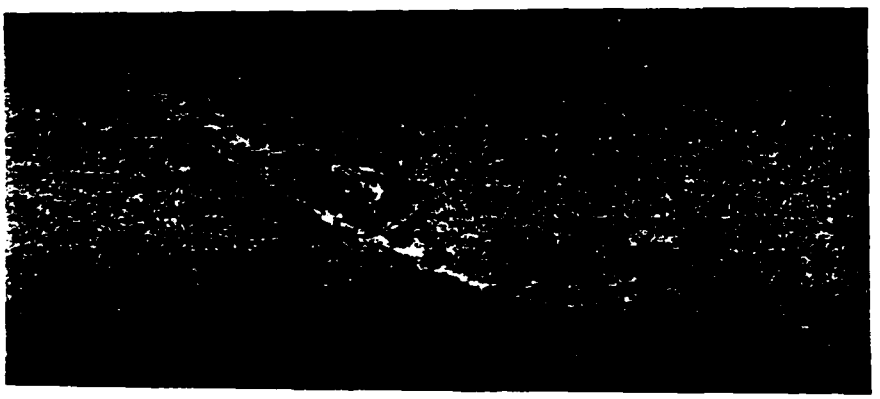

c) - 4 Depths of Focus

Figure 19. Examples of SAR Imagery Made Using Different Azimuth Focus Corrections During Optical Processing (Rev. 651 Data)

7
RELATIVE RADAR BACKSCATTER MEASUREMENTS

In order to more rigorously analyze the relationship between the observed SAR surface features and corresponding bathymetric information, measurements of the radar backscatter return were compared to water depth profiles. These measurements were obtained in two ways. Backscatter measurements were obtained by placing a scanning device in the output plane of the optical processor. The output plane of the optical processor is the position where the film (output) is placed to record the output imagery. Scanning at the output plane of the processor enables one to avoid the log transformation of a film, and also retain the full dynamic range of an image. The scanning device used in this study utilized a source aperture that corresponded to an ocean area of 350 x 350 M. This technique requires the use of SAR signal histories of a study area. The other method for obtaining backscatter measurements was through the use of JPL digitally processed CCT data. For convenience, the backscatter measurements were obtained in transect form, which could then be compared to the bathymetry of a test site. Optical processor scans were obtained for three of the study sites (A, D, E) and JPL CCT data was used on Study Site C.

It should be noted that radar backscatter values presented in this section are relative radar backscatter values. The SEASAT SAR was not calibrated in terms of producing actual σ_o radar cross section values. The relative radar backscatter scans have not been corrected for affects of antenna, range power loss, sensitivity time control (STC), or resolution size. These corrections are rather time consuming, but should be considered in future evaluations.

Figure 20 summarizes the relative radar backscatter measurements made in the optical processor of Study Site A, located near Bimini Island. In Scan 1, we can see an almost 50% increase in relative radar backscatter when we compare the deep water area with the shallow water area. In Scan 2, we note a gradual increasing trend as we pass from deep to shallow water, but the difference in backscatter measurements between deep and shallow water is not as dramatic as with Scan 1. The ocean process responsible for the difference between Scan 1 and 2 is not well understood at present. Speculations as to the cause of the differences between Scan 1 and 2 will be discussed in the next section.

Figure 21 summarizes the optical processor backscatter scans made for sub-site 1 of Study Site D (the Thames River Estuary region), and Figure 22 summarizes the scans made for sub-site 2 (the English Channel region). Both sets of scans show a close correlation between a surface signature (a sharp rise or drop in backscatter) and a distinct water depth change. It should be noted that these scans were made from non-geometrically corrected imagery, and as such, only represent approximate correlations. In Figure 21, a sharp increase in water depth is associated with an increase in backscatter. In Figure 22, a decrease in water depth is associated with an increase in backscatter. In scan a of Figure 22, a slight backscatter drop occurs just prior to the sharp rise over the shoals.

Figure 23 summarizes the optical processor backscatter made at Study Site E. We have already noted the close correlation between the SAR observed surface features and the bathymetry of this area (see Figure 15). It should be noted that the very large peaks in Scans B and D of Figure 23 are from North Rona Rock, and do not represent an ocean surface variation. It is clear from Figure 23, however, that the relative backscatter from the shoal area is higher than from the surrounding deep water areas (i.e., as the water depth decreases, the backscatter increases). The underlying oceanographic processes responsible for the backscatter variations (noted above) over the shoal regions are not yet understood completely.

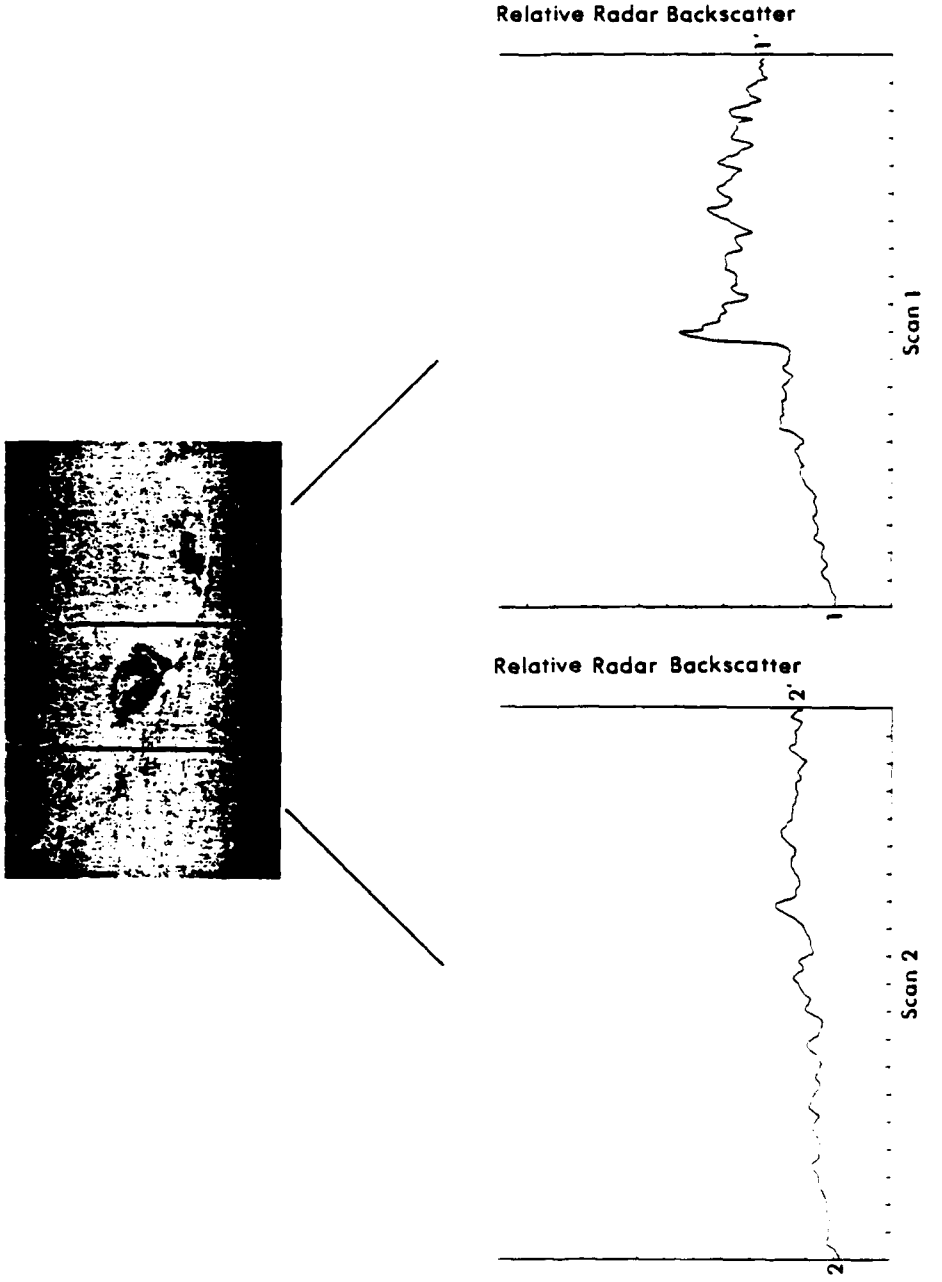

Figure 20. Summary of Relative Backscatter Measurements Made at Study Site A (Bimini Island) from SEASAT Rev. 651, 19 August 1978.

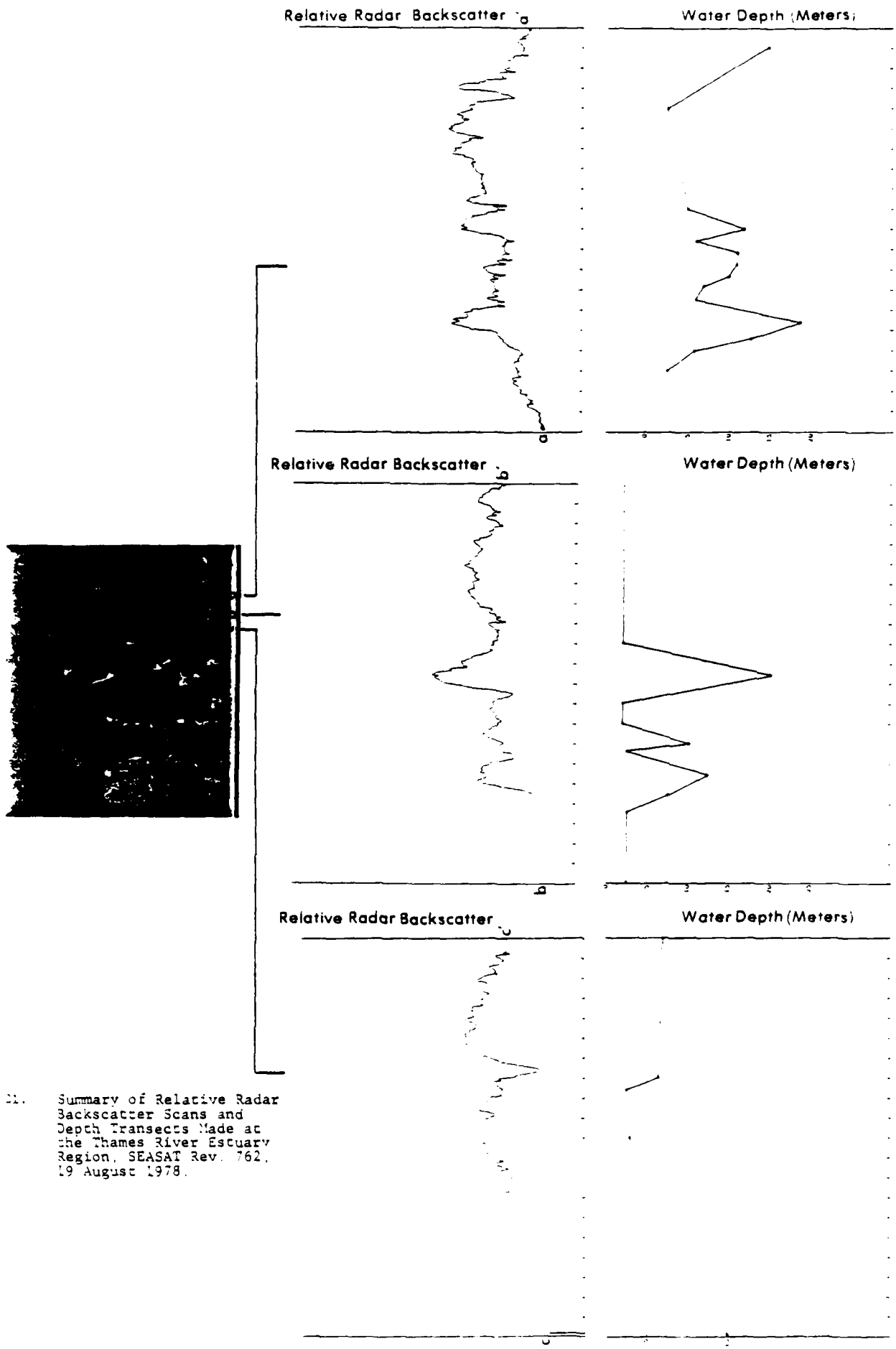

FIGURE 11. Summary of Relative Radar Backscatter Scans and Depth Transects Made at the Thames River Estuary Region, SEASAT Rev. 762, 19 August 1978.

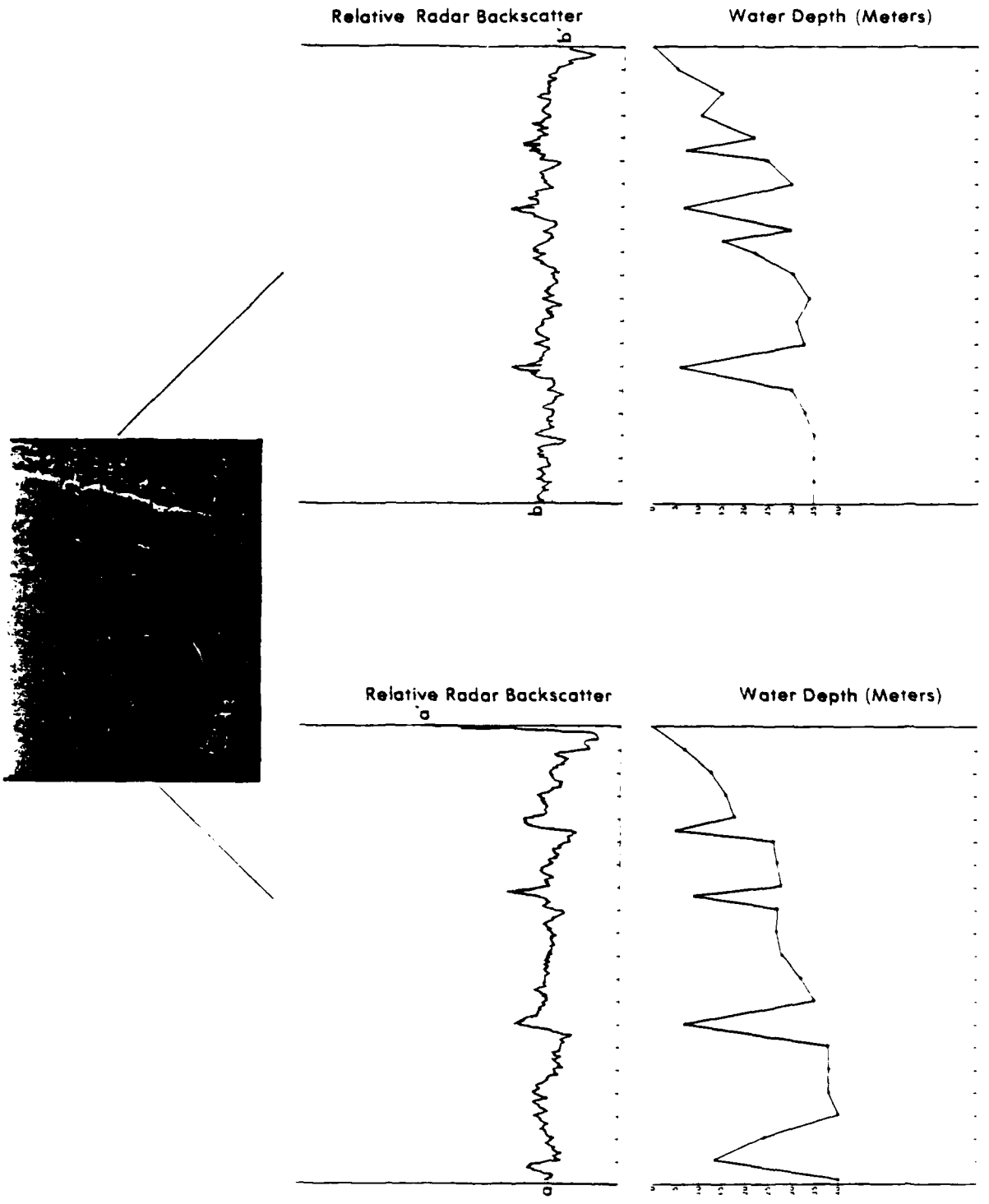

FIGURE 11. Summary of Relative Radar Backscatter Measurements and Depth Transects Made at the English Channel Region, SEASAT Rev. 762, 19 August 1978.

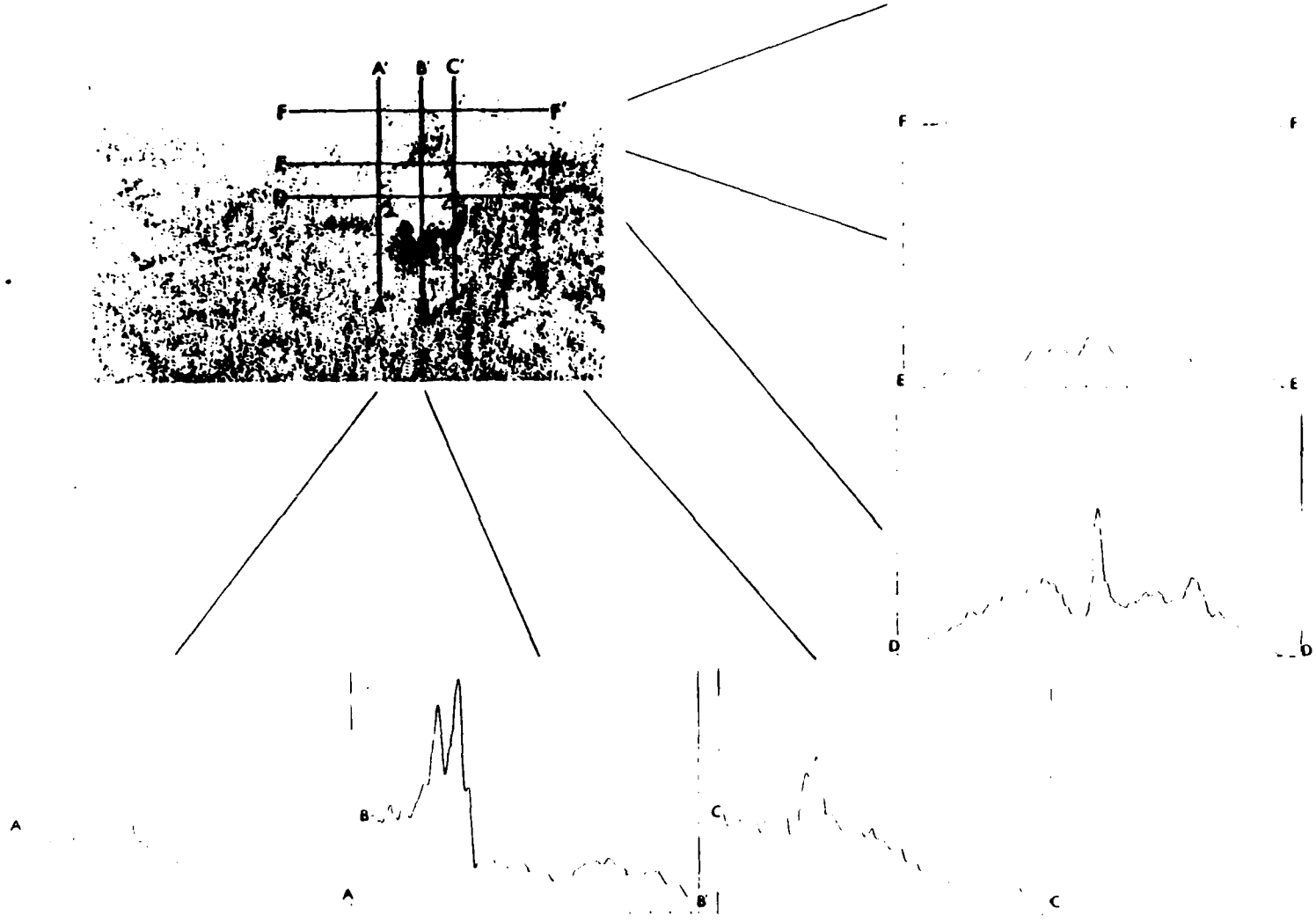

FIGURE 23. Summary of Relative Radar Backscatter Measurements made at Study Site E (North Rona Rock) from SEASAT Rev. 762, 19 August 1978

The JPL digitally processed SAR image from Nantucket Island (Revolution 880) is shown in Figure 24. The data has 25 m resolution and represents an area of 100 x 100 km. If Figure 24 (a positive print) is compared to Figure 6, a photographic negative of JPL optically processed SAR data, the better quality of Figure 24 is apparent.

Figure 25 shows the location where relative radar backscatter measurements were digitally obtained.

The digital processing consisted of extracting 5 lines of data at each of the shown transects. These were then averaged to form a single line, which in effect was smoothing the data in the azimuth dimension. Geometric corrections were then performed using techniques outlined by Shuchman, et al. (1978). Appendix B presents a summary of the geometric correction used along with a verification of the algorithm. Next, the data was low-pass filtered utilizing a variable aperture sliding window technique to smooth the data in the range direction. These scans were then all normalized by subtracting from each pixel the maximum value obtained and converting them to dB. Bathymetry cross-sections were also produced corresponding geographically to the backscatter transects. The bathymetry cross-section data were obtained from NOAA Chart No. 13237.

The digital backscatter transects and bathymetric cross-sections are shown in Figures 26-28. Examination reveals an inverse correlation of backscatter return and water depth, that is, the larger the depth, the smaller the corresponding backscatter, and vice versa. It can be observed from Figures 26-28 that the correlation of radar backscatter appears to be quite good. In general the radar signal increases 3 dB (i.e., a factor of two) over the topographic ridges present on the sea floor in the Nantucket Shoals area. The profiles presented in the figures indicate that the radar backscatter

FIGURE 24. SAR Imagery made from JPL Produced Digital Data, Nantucket Island, SEASAT Rev. 380, 27 August 1978

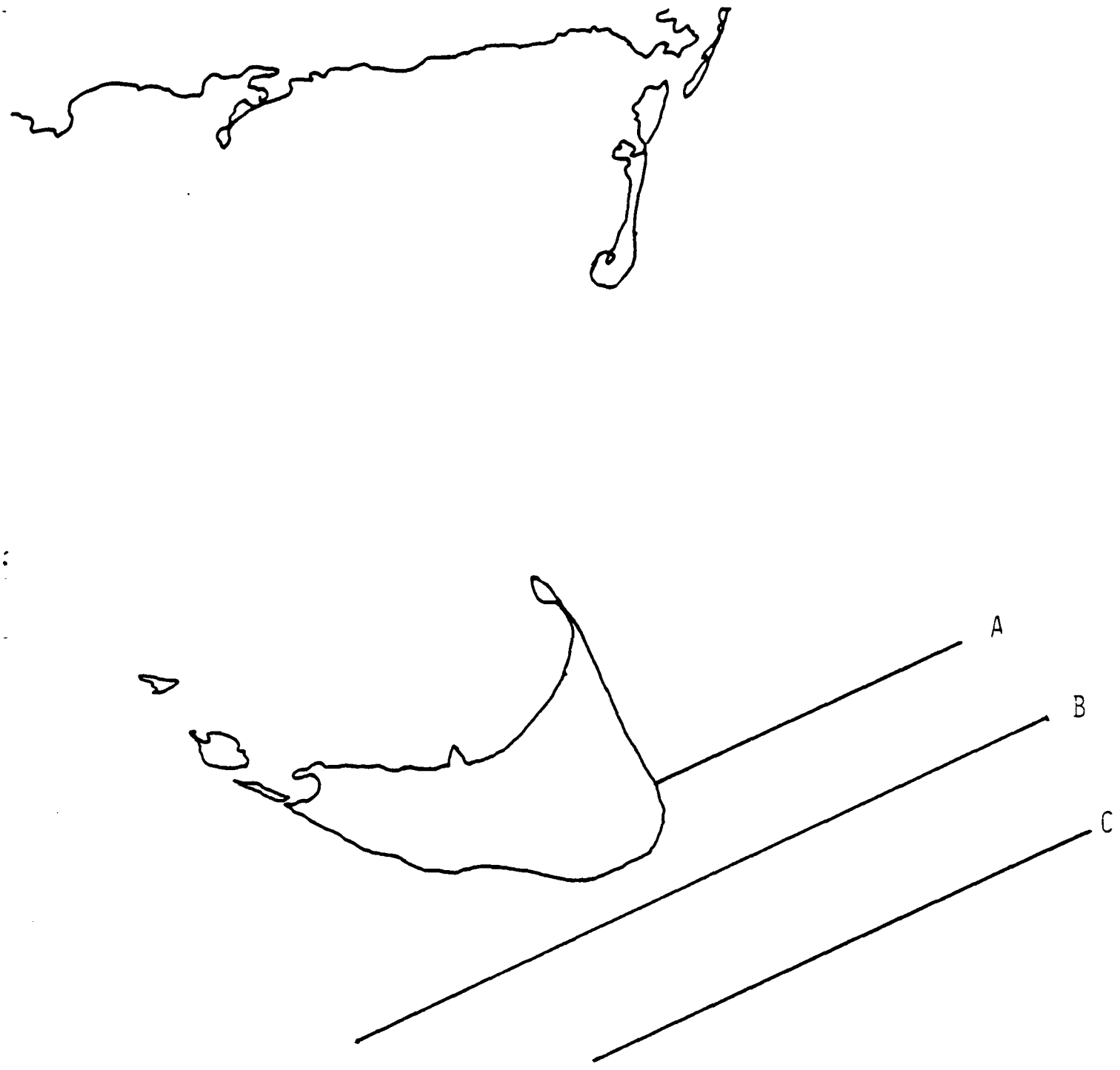

FIGURE 25. Location of Relative Radar Backscatter Measurement Transects for Rev. 880 Data

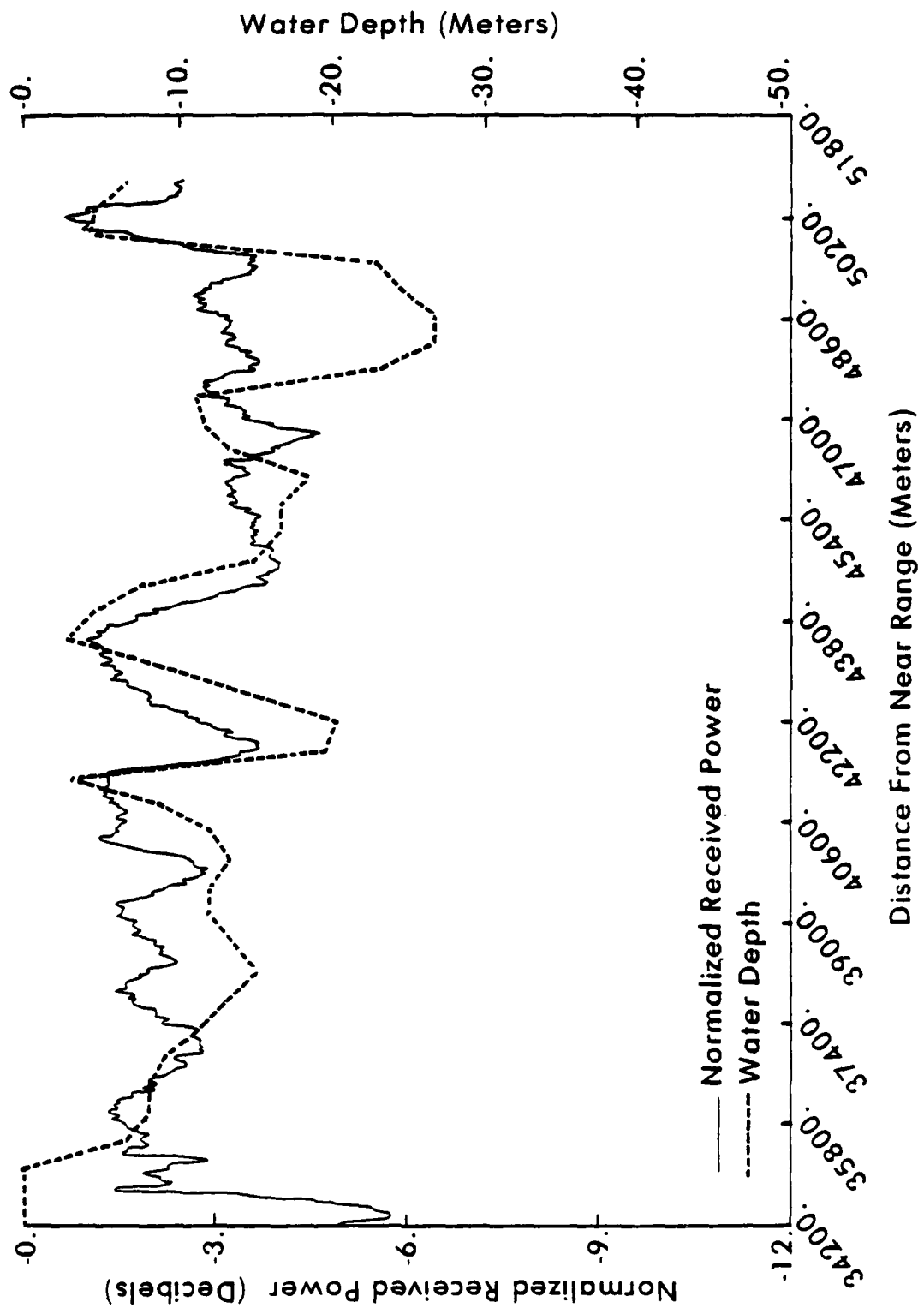

FIGURE 26. Relative Radar Backscatter Measurements and Depth Transects for Scan A, Nantucket Shoals, SEASAT Rev 880, 27 August 1978.

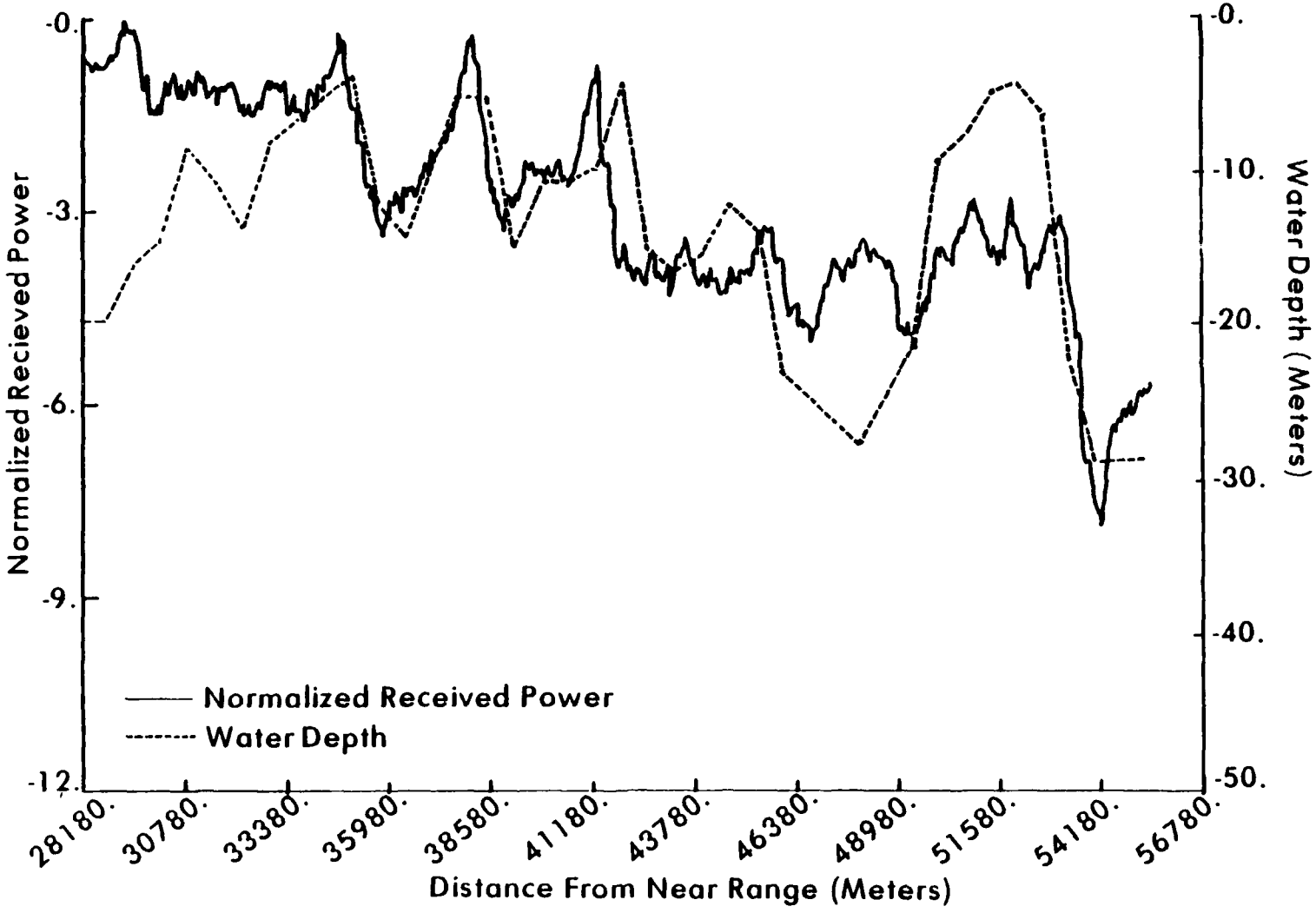

FIGURE 27. Relative Radar Backscatter Measurements and Depth Transects for Scan B, Nantucket Shoals, SEASAT Rev. 880, 27 August 1978.

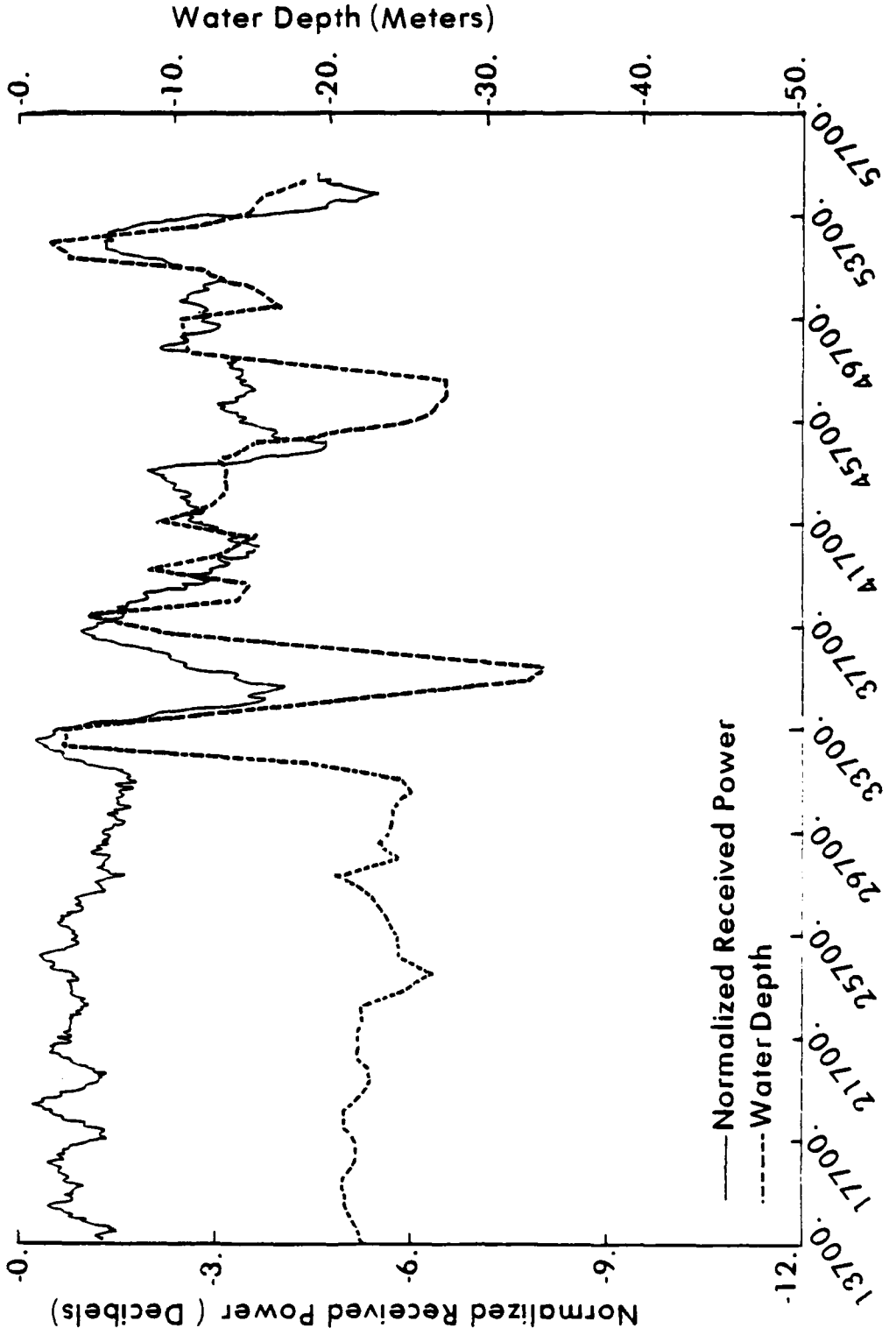

FIGURE 28. Relative Radar Backscatter Measurements and Depth Transects for Scan C, Nantucket Shoals, SEASAT Rev. 880, 27 August 1978.

value increases directly above the topographic ridges, as opposed to slightly preceeding or following the position of the ridge. Unfortunately, the accuracy limitations of the bathymetric chart prevented the above posed theory from being examined in greater detail.

Plans are currently being finalized to further study the surface features observed in the Nantucket Shoals area. This experiment (named SEBEX for Surface Expression of Bathymetry EXperiment) will bring together oceanographers as well as SAR engineers to investigate both the spatial occurrence of these features as well as the SAR/sea surface interactions which cause them.

8

DISCUSSION

This study has shown that, in the limited number of areas studied, SEASAT synthetic aperture radar (SAR) image signatures can be related to bottom topographic features. The depth related surface signatures appear to be present on the SAR data only when currents or gravity waves are present. Additionally, the orientation of the waves or currents in respect to the bottom feature appears to be important. The effect of local wind (including orientation and magnitude) on the visibility of bottom related signatures on SAR imagery is not known at present and needs to be studied in detail. It is known, however, that a minimum wind (on the order of 6 knots) is needed to generate the capillary wave field responsible for radar backscatter from the sea surface.

The SAR signatures are believed to be an indirect result of a hydrodynamic interaction between an ocean process (or air/ocean process) and the bottom shapes and depth features. This concept can be better understood if an example is presented where a distinct ocean process results in an alteration of the sea surface, which in turn can be imaged by a satellite sensing system such as SEASAT. The illustration used will be the internal waves presented earlier in Figure 1. Figure 29 shows a schematic (after LaFond and Cox, 1962) where part of the energy field from an internal wave is being transmitted towards the surface. This energy in turn creates an area where the sea surface is rougher than adjacent areas. An area of increased roughness is caused by the interaction between the internal waves and the surface capillary waves. The internal wave energy at the ocean's surface causes a "bunching" of the capillary waves. This bunching of the capillary waves creates a situation where there are more radar backscatterers per unit area than in adjacent areas, thus the increase roughness of this area. The altering rough-smooth pattern on the ocean's surface (above the internal wave) can then be imaged by the SEASAT SAR, as they were in Figure 1. This basic concept (that an ocean process can result in altering the surface roughness to a degree which is detectable on SAR imagery) can be expanded to include effects such as currents and gravity wave motion.

Compression of Surface Layers

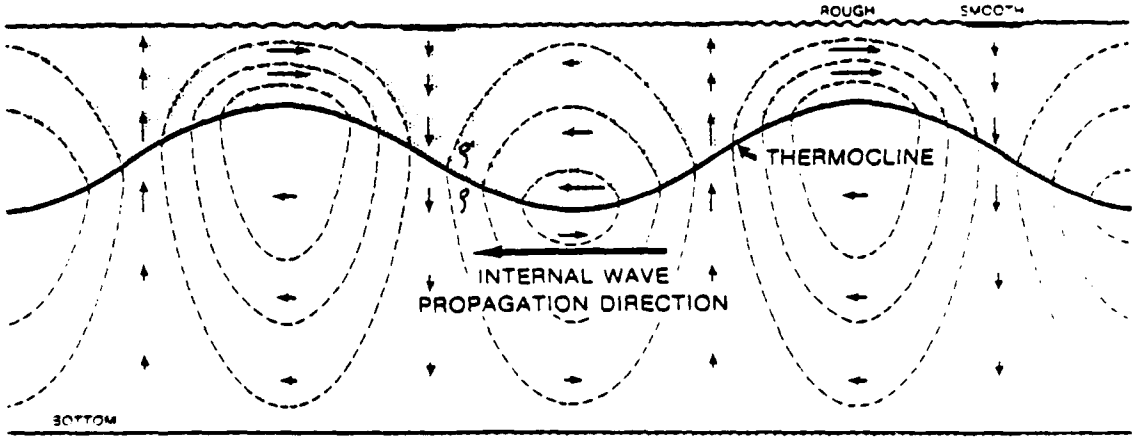

FIGURE 29. Schematic of the Structure of Progressive Internal Wave Motion Along a Sharp Thermocline Illustrating Alteration of Surface Roughness (after Lafond and Cox, 1962)

The principle in imaging any ocean surface with a radar is that the backscatter of microwave energy (echo) received by the radar receiver contains information on the roughness characteristics (shapes, dimensions, and orientations) of the reflecting area. Parameters that influence the radar return received from ocean surfaces include the motion of the scattering surfaces, the so-called speckle effect, system resolution and non-coherent integration, as well as contributions attributable to wind, waves, surface currents and surface tension.

The final output of a SAR system is usually in the form of a two-dimensional display of relative radar backscatter intensity. The basic backscattering mechanism is believed to be Bragg scattering (Wright, 1966); that is, transmitted radar energy with wave number K interacts in a resonant fashion with ocean surface waves with wave number K_w such that

$$K_w = 2K \sin \theta, \qquad (2)$$

where $K_w = 2\pi/L$ and $K = 2\pi/\lambda$ are the wave numbers and L and λ the wavelengths, respectively, of the surface waves and the radar, and θ is the incidence angle. For the SEASAT parameters, the Bragg wavelength is between 30 and 40 centimeters. Shuchman, et al. (1978a) showed that a Bragg-Rice scattering equation satisfactorily explained the radar backscatter return from SAR using data collected during the Marineland experiment (Shemdin, et al., 1978). It should be noted that radar data from large ocean areas (1 x 1 km) were averaged in that analysis. Thus (based on the above), the principle radar reflectivity mechanism of imaging ocean surfaces is via capillary and small gravity waves (Raney and Shuchman, 1978). Any alteration of the structure of these waves will result in a backscatter variation in the recorded signal histories.

In the following discussion, we will present some of the proposed theories that attempt to explain the SAR signatures observed in each of the test sites. This section of the report cannot be considered complete as all proposed theories are not presented, and much more work is necessary in this area. The SAR data cannot be effectively used as an

indicator of bottom topographic information until the limitations of the SAR data are understood. The limitations of using SAR imagery to obtain topographic information by SAR will be best understood by development of a theory of the imaging mechanism.

The least distinctive (in terms of bottom bathymetry) signatures occurred in the SAR imagery from Sites A and B, which were located in the Bahama Island group. The only surface patterns which were believed to be bathymetrically related are along the edge of either the Little or Great Bahama Banks where the bathymetry goes from shallow to very deep water over a short ground distance. In no case was the entire edge of either of these banks reflected on the SAR imagery.

A possible mechanism for the presence of SAR signatures in these study sites lies in the SAR's ability to detect surface currents (see Shuchman, et al., 1979a). An example is the nearshore region near Bimini Island (see Figure 8), where a one to two knot (0.5 to 1.0 m/s) northerly current exists as a result of the Gulf Stream. Because of the Banks, this current would not extend eastward due to frictional forces, and this current differential (or current shear) is then detected on the SAR imagery.

Only the western portion of the Great and Little Bahama Banks have been studied here. In this area, very few distinct bottom features exist (other than the islands and shoals along the edges of these bands and a sharp drop-off at their edges). Consider the above observation with the absence of significant tidal currents (probably less than one-half knot or .25 m/s), at the time of the SEASAT overpasses, and a situation exists where there is little possibility for an interaction between a bottom feature and an ocean process to occur. Other authors have reported the presence of distinct bottom features on Landsat imagery (Hine, 1977 and Defense Mapping Agency, 1980), and on SEASAT imagery (Sherman, 1980).

An example of one such area is presented in Figure 30, which is from SEASAT Rev 1411, collected on 3 October 1978. Figure 30 was collected over the Tongue of the Ocean, a prominent deep water trench which extends into the Little Bahama Bank. As can be seen, prominent surface features

exist, which are believed to be bottom related. SEASAT made at least five passes over this area and this represents a study site for future studies.

As noted earlier from Figures 21 and 22, we have two opposite situations occuring at Site D. In the Thames Estuary Region (Figure 21) an increase in water depth is associated with an increase in backscatter. In the English Channel Region, a decrease in water depth is associated with an increase in backscatter. One would expect that two separate oceanographic/bottom interactions are responsible.

When interpreting SAR ocean imagery, one associates a decrease in radar backscatter with decreased water-surface roughness and vice-versa. The Thames River Estuary is an area of very shallow (<1m) tidal flats and it is quite possible that the capillary waves over these flats are sufficiently suppressed to result in a significant decrease in surface roughness.

The backscatter variations observed in the English Channel sub-site are believed to be tidal current induced. The exact mechanics of these tidal overfall areas will be discussed in greater detail below. Figure 31 shows the tidal currents which were present during the SEASAT Rev. 762. Note that 1 to 2.5 knot (0.5 to 1.25 m/s) currents existed. Unfortunately, the wind conditions on the day of the overpass are not known at the time of this writing. Figure 32 is from a Landsat study of the Test Site D performed by Viollier and Baussart (1979). Of particular interest to this study is the MSS Band 7 (800 to 1100nm) imagery in which there is essentially no penetration into the water column and hence any patterns over water are the result of the sun's reflection off the capillary waves on the water surface. In the 12 June 1975 Band 7 imagery (on Figure 32), the same linear patterns are present in the center of the English Channel as were present in the SEASAT imagery (Figure 12) of the same area. Tidal current conditions were essentially the same during the collection of the 12 June 1975 Landsat and the Rev. 762 SEASAT data, with a strong tidal flow to the southwest. The 30 March 1977 Landsat imagery in Figure 32 was collected at a time when the tidal flow was opposite in direction (towards the northeast) to

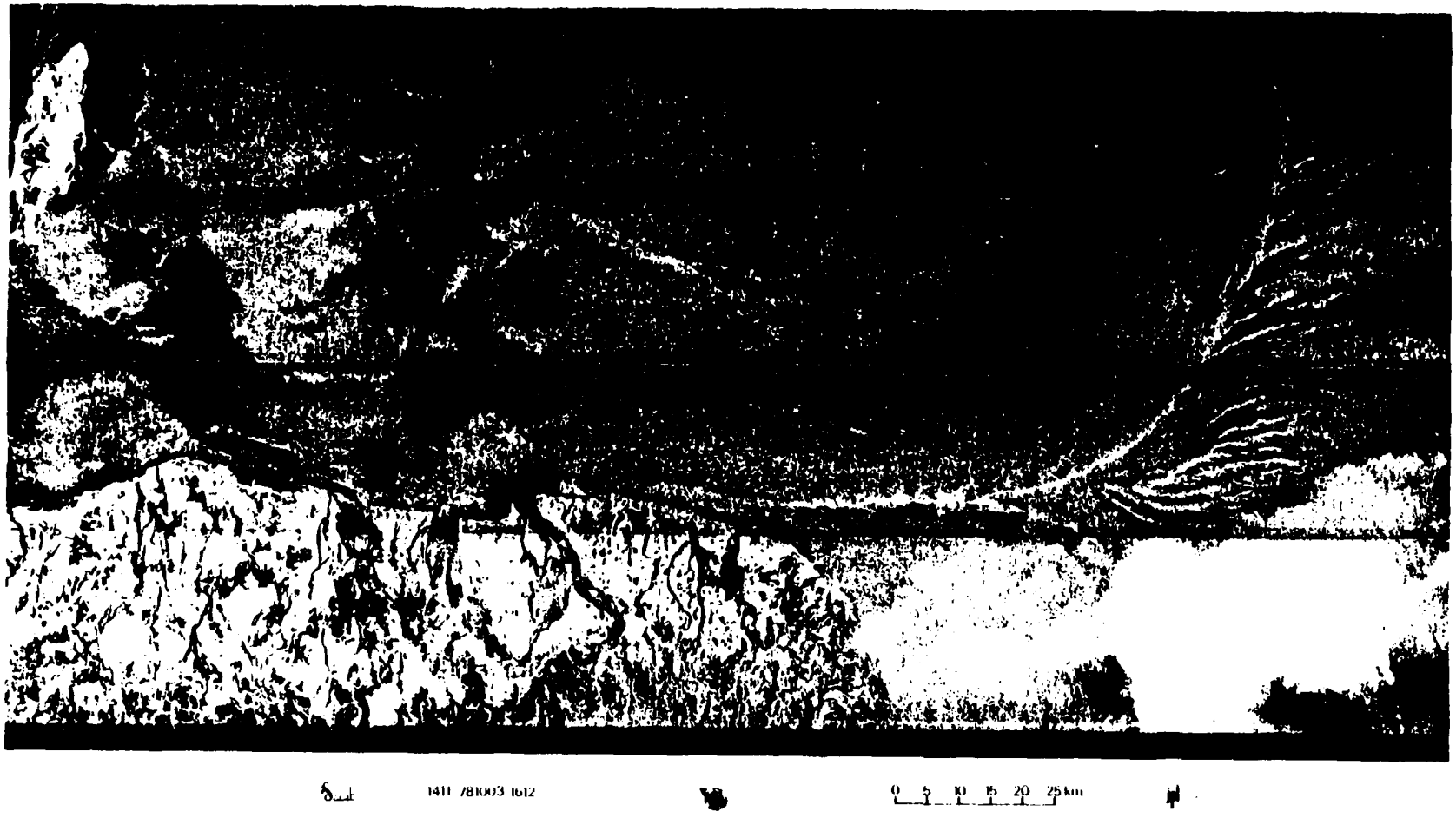

FIGURE 30. SEASAT REV 1411 OVER THE TONGUE OF THE OCEAN (BAHAMAS).

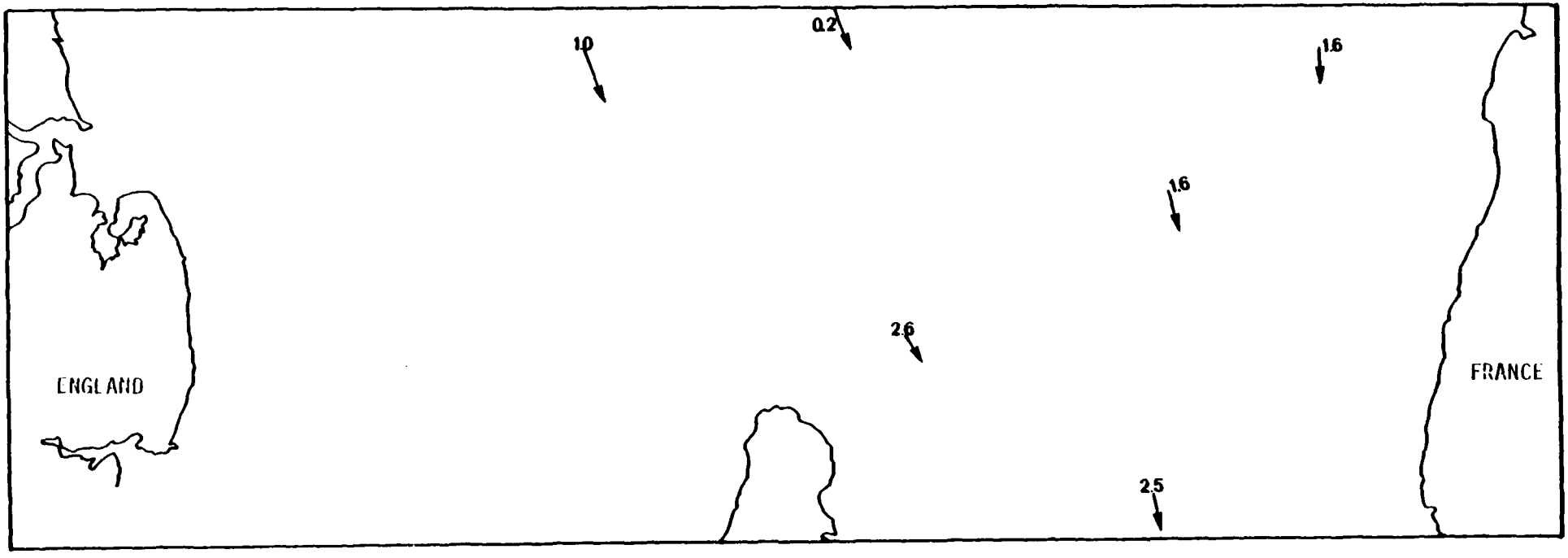

FIGURE 31. Summary of Tidal Current Velocities at the Time of SEASAT Rev. 762 over the English Channel, 19 August 1978 (velocities are in knots, 1 knot = ½ meter/second).

12 JUNE 1975

30 MARCH 1977

MSS 5 (600-700 nm)

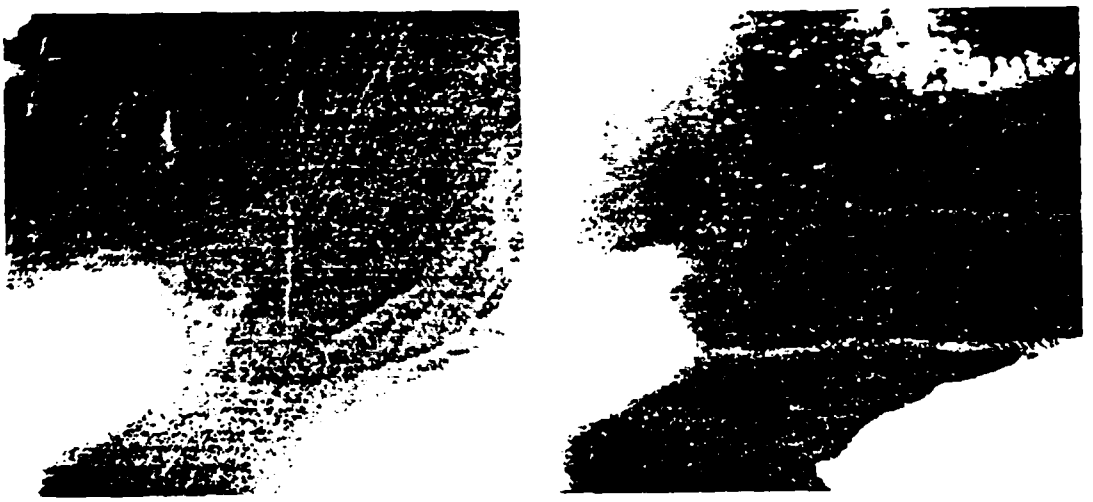

MSS 7 (800-1100 nm)

FIGURE 32. Landsat Imagery of Study Site D, Sub-site 2 (English Channel) (from Wollier and Baussart [1979] with permission of the authors)

the tides present on 12 June 1975. No depth related signatures can be observed on the 30 March 1977 Landsat data. It should be noted that very little wind was present during the March imagery and the sun illumination was low, a poor set of conditions for sun glitter off the water.

The Landsat imagery from this study is important from several standpoints. It indicates that the depth related features observed on the SEASAT imagery were not just coincidental to the time of the SEASAT overflight. Also, the comparison of Landsat imagery from two dates when opposite tidal flows and different wind conditions were present shows the necessity of a distinct oceanic physical process in order that the bottom related surface feature be present on the imagery.

The possible mechanism for the surface features in the shoal areas around North Rona Rock (Study Site E, see Figures 14 and 15) is not yet clear, but their occurrence directly over a shoal area which is surrounded by deeper water leaves very little doubt that they are related to the bottom bathymetry of the area.

One possible mechanism for the presence of surface anomalies on SAR imagery over North Rona Rock is a non-linear interaction between gravity waves and surface capillary waves due to the sharp rise ($\sim$40 meters) in the bottom in the shoal region. This sharp rise causes a drastic alteration in the gravity wave structure which results in both wave refraction and a gravity-capillary wave interaction. The surface signatures might possibly be tidal-current induced, although the tides in this area at the time of the SEASAT overpass were probably less than one-half knot (.25 m/s) in an easterly direction.

Figure 33 summarizes the tidal and wide conditions present at the time of the SEASAT Rev. 880 over Nantucket Island (Study Site C). Weather records were consulted to see if any major climatic events occurred on or before the SEASAT overpass. The region was dominated

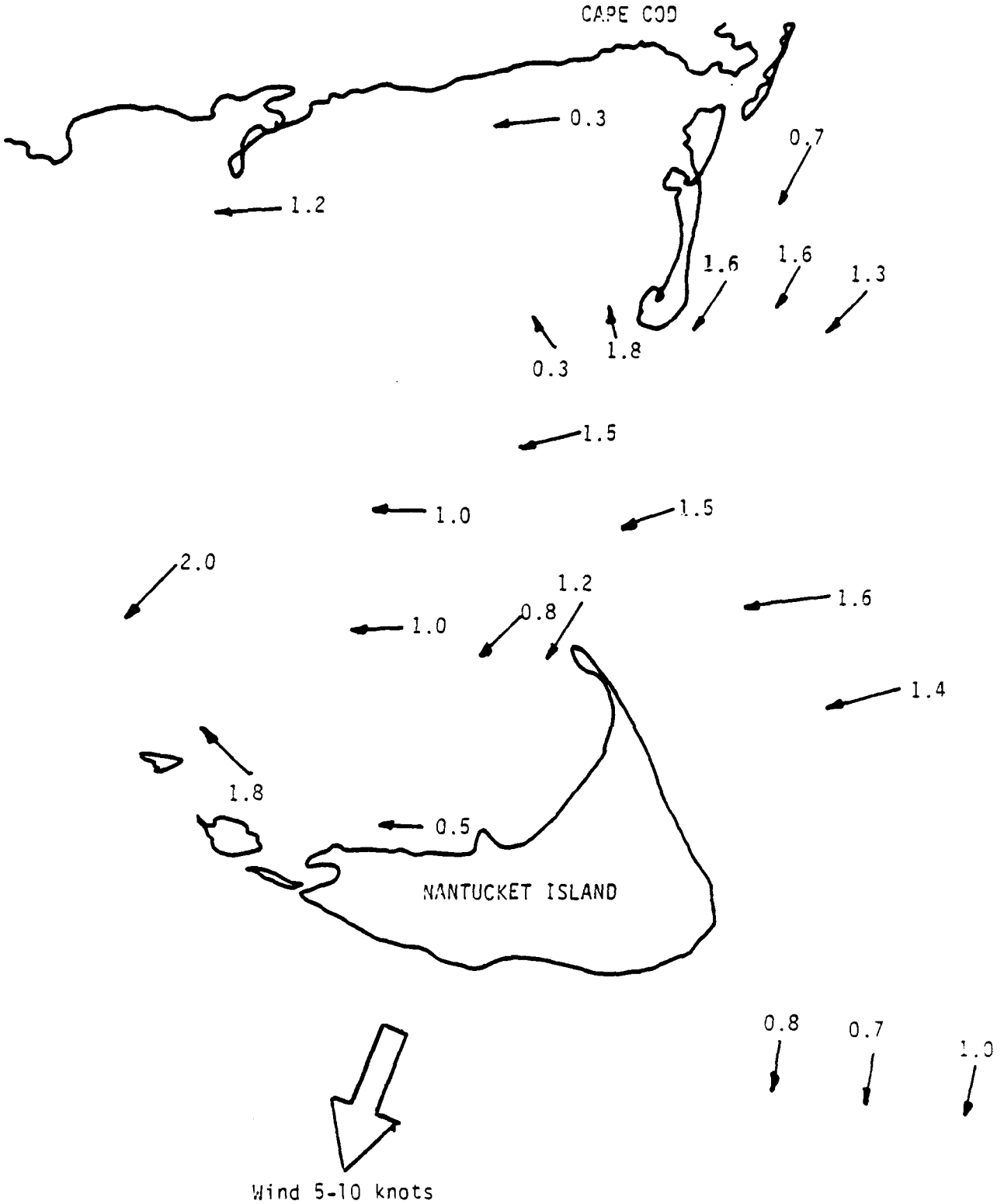

FIGURE 33. Summary of Tidal Current Velocities and Wind Speed in the Nantucket Island Area at the Time of SEASAT Rev. 880, 27 August 1978 (velocities in knots, 1 knot = ½ meter/second).

by a high pressure center during and several days prior to the SEASAT overpass. Wind speeds were generally light, in the range of 5-10 knots (2.5 to 5.0 m/s) from the north.

It is believed that the surface patterns in the inshore regions of Rev. 880 are the result of an interaction between the tidal currents and the shoals in the Nantucket Island/Cape Cod region. This notion is again supported by observations made from Landsat imagery. Figure 34 is a Band 6 (.7-.8 μm) image collected on 17 July 1974. Like Band 7, Band 6 has very little water penetration, and therefore, water features present on the imagery are a result of reflected sunlight from the capillary waves on the ocean surface.

The relative radar backscatter scans (Figures 26-28) made for this area showed the close correlation between backscatter and water depth in this area. The scans could not positively answer the question whether the increase in radar backscatter (associated with a decrease in water depth) occurred over the topographic "bump" in bottom or slightly preceeding or after the features. It is assumed that the large rise in radar backscatter observed on the Nantucket Shoals data occurs slightly after the ridge in bottom. The oceanographic cause of the increase in backscatter is commonly referred to as a tidal overfall and has been well documented by Stewart and Jordan (1964). Stewart and Jordan studied the underwater and ridges of Georges Shoal which is located approximately 120 km east of the Nantucket test area. The Georges Shoal is very similar to the Nantucket Shoals in that an elongated bank of shallow water (over the shoals) lies next to an area of deeper water (usually 10 to 15 meters deeper). Stewart and Jordan reported that when a strong (in excess of 1-1/2 kts or 1m/s) tidal current flowed normal (perpendicular) to the ridges on Georges Shoal, an overfall is created as the large volume of fast moving water is forced upward and over the ridge. An actual rise of the sea surface was observed by Stewart

FIGURE 34. Band 6 Landsat Imagery of the Cape Cod/Nantucket Island Area, Collected on 17 July 1974

and Jordan just down current from the crest of the underwater ridge. The overfall "wave" was stationary relative to the bottom feature which was creating it (along with the tidal current). These overfall waves were only present during times when the tidal currents were strong and normal to the ridges. The overall waves are short-period waves and, typically, a short period breaker line can develop (Stewart and Jordan, 1964).

From Figure 33, it is clear that the tidal currents are generally perpendicular to the underwater topographic features. Therefore a similar situation to that reported by Stewart and Jordan (1964) could have occurred at this study site, which would account for the large scale surface features on the SAR imagery.

The observations made from the Landsat imagery in Figure 34 were also consistent with Stewart and Jordan's work. The tides on the date the Landsat data was collected were similar in magnitude and direction as at the time of the SEASAT overpass (Reed, 1980).

9
CONCLUSIONS AND RECOMMENDATIONS

This study has helped to demonstrate that synthetic aperture radar (SAR) data has the potential to detect bathymetric features in shallow water regions. The detection process is via a hydrodynamic interaction between currents and/or waves with the bottom topographic feature which alters the surface roughness of the ocean. The SAR is very sensitive to surface roughness changes of the ocean surface, and because microwave sensors, like SARs, do not penetrate more than a few centimeters into the ocean, the depth-related signatures are ocean surface effects.

The greatest potential exists for SAR detection of bottom features in areas where there are shoals with currents flowing over them. Presently, the SAR data can only be used as an indicator of shoal areas, but perhaps this information can be used to ascertain whether a bathymetric chart needs updating or revision. This could be done by correlating the SAR signatures to a digitized bathymetric chart. Whether a theory and a resulting processing algorithm can be developed that relates the radar backscatter signatures observed in this report directly to actual water depth is not known, and should be an area of future research.

Areas where distinct bathymetric features occur in coastal areas and in which physical oceanic processes occur (strong current or wave action) present the best potential for bathymetry/SAR correlations. In the present study, the Nantucket Shoals, English Channel, Thames River Estuary and North Rona Rock shoals represented such areas. Although portions of the edge of the Bahama Banks were discernible

on the SAR imagery, bathymetric information on the Banks themselves was not; this was most likely due to the lack of a physical oceanic process or a distinct bathymetric feature. Recalling that the banks are relatively flat, even if currents or waves were present, they need to interact with a bathymetric feature, which is not present. Special photographic enhancement and optical processing techniques did not seem to add any information in the Bahama Banks area.

Digitally processed SAR data offers the greatest potential in further research because this form of data lends itself to computer processing techniques. Computer processing is necessary to geometrically and radiometrically correct the large volume of information present in SAR data sets. Geometric correction of the data is necessary for accurate comparison with localized bathymetry data.

Many anomalous surface features occur on SEASAT imagery collected over deep ocean areas. Care must be taken when interpreting the significance of these features in relation to bathymetric information. Extensive study of physical oceanic processes and their SAR signals have yet to be conducted. Investigators of coastal area remote sensing imagery must be cautious in interpreting SAR imagery in order that the data are correctly analyzed.

This study consisted of a limited data set in that only a few oceanographic areas were analyzed. Additionally, all the various techniques available to study the data were not used at each test site. Further research needs to be explored to more fully exploit the use of SAR data for the detection of shallow water bathymetric features. They include:

a) examination of other SEASAT SAR passes of coastal regions to observe topographic bottom features;

b) examination of other SEASAT SAR passes of the five test sites used in this study. Hopefully SAR data was collected over the five sites during different environmental conditions (i.e., different wind, wave and current conditions). These additional data sets could be used to better define the limitations of SAR sensing of topographic features.

c) utilization of more sophisticated analysis techniques on test areas that show particular promise.

Specifically further research in the use of SEASAT SAR data to detect shallow-water features should include:

a) the quantification of environmental parameters (such as wind, wave and tide information);

b) geometric and radiometric (power loss, antenna patterns, sensitivity time control) corrections of the SAR data;

c) computer merging of the SAR data with bathymetric data to statistically correlate the relationship between the two;

d) merging of SEASAT data with Landsat data;

e) merging and/or comparing SEASAT data from the same area from different dates;

f) based on the above, explore the development of theories and algorithms to define the relationship between SAR detected surface features and bottom topographic information.

REFERENCES

Brown, W.J. and L. Porcello, An Introduction to Synthetic Aperture Radar, IEEE Spectrum 6, pp. 52-66, 1969.

Defense Mapping Agency, Berry Islands, The Bahamas, SATELLITE IMAGE MAP, NASA Landsat-2, 1:500,000, N2600W07752, DMA Hydrographic/ Topographic Center, Washington, D.C., 1980.

DeLoor, G.P. and H.W.B. Van Hulten, Microwave Measurements Over the North Sea, Boundary Layer Meteorology 13, pp. 119-131, 1978.

Doak, E., J. Livisay, D. Lyzenga, J. Ott and F. Polcyn, Evaluation of Water Depth Techniques Using Landsat and Aircraft Data. ERIM Final Report No. 135900-2-F. Ann Arbor, Michigan, 1980.

Harger, R.O., Synthetic Aperture Radar Systems, Academic Press, New York, 1970.

Hine, A.C., Lily Bank, Bahamas: History of an Active Oolite Sand Shoal, Journal of Sedimentary Petrology: 47(4), pp. 1554-1581. 1977.

Kozma, A., E.N. Leith, and N.G. Massey, Titled Plane Optical Processor, Applied Optics, 11, p. 1766, 1972.

Larson, R.W., P.L. Jackson, R.J. Dallaire, R.A. Shuchman and R. Rawson, Interpretation and Measurement of Multichannel Microwave SAR Imagery, Proc. of the Tenth Inter. Symp. Rem. Sens. Environ., pp. 53-66, 1975.

LaFond, E.C. and C.S. Cox, Internal Waves, The Sea, Vol. 1, M. N. Hill (Ed.), Interscience Publishers, New York, pp. 731-763, 1962.

Lyzenga, D.R., Shallow-water Reflectance Modeling with Applications to Remote Sensing of the Ocean Floor, Proc. of the Thirteenth Inter. Symp. on Rem. Sens. Environ., pp. 583-602, 1979.

Raney, K. and R.A. Shuchman, SAR Mechanisms for Imaging Waves, Proceedings of the 5th Canadian Symposium on Remote Sensing, Victoria, 1978.

Reed, C. 1980. Interpretation of Hydrographic Features in the Waters off Cape Cod, University of Mich. Masters Thesis (in preparation), Ann Arbor, Michigan, 1980.

Shemdin, O.H., W.E. Brown, Jr., F.G. Staudhammer, R. Shuchman, R. Rawson, J. Zelenka, D.B. Ross, W. McLeish and R.A. Berles, Comparison of In-Situ and Remotely Sensed Ocean Waves Off Marineland, Florida, Boundary Layer Meteorology, Vol. 13, pp. 225-234, 1978.

Sherman, J.W., III. Personal communication.

Shuchman, R.A., P.L. Jackson and G.B. Feldkamp, Problems of Imaging Ocean Waves with Synthetic Aperture Radar, ERIM Report No. 124300-1-T, Ann Arbor, Michigan, 1977.

Shuchman, R.A. and J.S. Zelenka, Processing of Ocean Wave Data from a Synthetic Aperture Radar, Boundary Layer Meteorology 13, pp. 181-191, 1978.

Shuchman, R.A., R.B. Innes, C.L. Liskow, B.T. Larrowe and A. Klooster, ERIM SEASAT SAR Engineering Evaluation, ERIM Technical Report No. EM-79-1024, Ann Arbor, Michigan, 1978.

Shuchman, R.A., A. Klooster and A.L. Maffett, SAR Mechanism for Imaging Ocean Waves, Proceedings EASTCON '78 Record, IEEE Electronics and Aerospace Systems Convention, 1978a.

Shuchman, R.A. and E.S. Kasischke, The Detection of Oceanic Bottom Topographic Features Using SEASAT Synthetic Aperture Radar Imagery, Proc. of the Thirteenth Inter. Sym. on Rem. Sens. Environ., pp. 1277-1292, 1979.

Shuchman, R.A., E.S. Kasischke, A. Klooster and P.L. Jackson, SEASAT SAR Coastal Ocean Wave Analysis: A Wave Refraction and Diffraction Study, ERIM Final Report 138600-2-F, Ann Arbor, Michigan, 1979.

Shuchman, R.A., C.L. Rufenach and F.I. Gonzales, The Feasibility of Measurement of Ocean Surface Currents Using Synthetic Aperture Radar, Proc. of the Thirteenth Inter. Sym. on Rem. Sens. of Envirn., Ann Arbor, Michigan, 1979a.

Stewart, H.G., Jr. and G.F. Jordan, Underwater Sand Ridges on Georges Shoal, in Papers in Marine Geology (Shepard Commemorative Volume) ed. by Robert L. Miller, The MacMillan Co., New York, pp. 102-114, 1964.

Teleki, P.G., R.A. Shuchman, W.E. Brown, Jr., W. McLeigh, D. Ross and M. Mattie, Ocean Wave Detection and Direction Measurements with Microwave Radars, Oceans, IEEE/MTS, Washington, D.C., 1978.

Viollier, M. and N. Baussart, Enhancement of Landsat Imagery for the Monitoring of Coastal Waters. Applications to the Southern Part of the North Sea, Proc. of the Thirteenth Inter. Sym. on Rem. Sens. Environ., pp. 1093-1105, 1979.

Wright, J.W., Backscattering from Capillary Waves with Application to Sea Clutter, IEEE Trans. Antennas Propagation, Vol. AP-14, pp. 749-754, 1966.

APPENDIX A

BATHYMETRIC CORRELATIONS

APPENDIX A

BATHYMETRIC CORRELATIONS

The first step in determining if SAR data could be used to provide bathymetric information was to determine whether or not the surface features observed on the SAR imagery occurred over or near distinct bathymetric features. This analysis was done through a procedure (termed bathymetric correlation) where a clear cell reproduction of a hydrographic chart (enlarged or reduced to the same map scale) was overlayed onto the SAR imagery. The water depth under each feature was then obtained from the chart, and this sub-feature depth was compared to the adjacent area (within a few hundred meters) water depth. It could then be determined if the feature on the SAR imagery occurred over or near an area where the water was shoaling or getting deeper.

For convenience, each Study Site was divided into a group of study areas. A study area is defined as the position on the SAR imagery where a feature believed to be bathymetrically related existed. After all these areas at a given Study Site had been identified, the clear cell reproduction of the chart of the Study Site was then overlaid onto the SAR imagery. The next step was to calculate the average water depth below each area marked on the SAR imagery. Then, the average depth of the water immediately adjacent to each study area was calculated. If the difference between these two averages were greater than 50 percent of the shallower depth, then a distinct bottom topographic feature was said to exist.

The bathymetric correlations for each Study Site (except Sites B [Southern Bahamas] and E [North Rona Rock]) are presented in Tables

A1 to A5. Because the number of study areas at Sites B and E were limited, no tables were constructed. Given in each table in this appendix are the Study Area, the Average Water Depth for both the Study Area and the Adjacent Area, and finally, a brief description from the SAR imagery of the characteristics of the study area versus the adjacent area.

TABLE A1. BATHYMETRIC CORRELATIONS FOR SITE A, DMA-BAHAMAS PHOTOBATHYMETRIC CALIBRATION AREA, SEASAT REV. 407

STUDY AREA	AVERAGE WATER DEPTH		WATER DEPTH DIFFERENCE	STUDY AREA COMPARISON WITH ADJACENT AREAS
	STUDY AREA	ADJACENT AREAS		
a	< 20 meters	>450 meters	430 meters	Study area a lighter toned, narrow line
b	< 20 meters	>450 meters	430 meters	Study area a lighter toned, narrow line
c	< 20 meters	>450 meters	430 meters	Study area a lighter toned, narrow line
d	>36\ ters	>360 meters	0 meters	Study area a lighter toned, narrow line
e	>360 meters	>360 meters	0 meters	Study area a lighter toned, narrow line

TABLE A2. BATHYMETRIC CORRELATION FOR SITE A, DMA-BAHAMAS PHOTOBATHYMETRIC CALIBRATION AREA, SEASAT REV. 651

STUDY AREA	AVERAGE WATER DEPTH		WATER DEPTH DIFFERENCE	STUDY AREA COMPARISON WITH ADJACENT AREAS
	STUDY AREA	ADJACENT AREAS		
a	< 20 meters	>450 meters	430 meters	Study area lighter toned, narrow line
b	< 20 meters	>450 meters	430 meters	Study area lighter toned, narrow line
c	< 20 meters	>450 meters	430 meters	Study area lighter toned, narrow line
d	> 360 meters	>360 meters	0 meters	Study area consists of various lighter toned, narrow lines
e	3 meters	8 meters	5 meters	Study area darker toned than surrounding adjacent areas

TABLE A3. BATHYMETRIC CORRELATION FOR SITE C, NANTUCKET SHOALS AREA, SEASAT REV. 880

STUDY AREA	AVERAGE WATER DEPTH		WATER DEPTH DIFFERENCE	STUDY AREA COMPARISON WITH ADJACENT AREAS
	STUDY AREA	ADJACENT AREAS		
a	5 meters	21 meters	16 meters	Study area lighter in tone than adjacent areas
b	4 meters	17 meters	13 meters	Study area lighter in tone than adjacent areas
c	4 meters	18 meters	14 meters	Study area lighter in tone than adjacent areas
d	3 meters	12 meters	9 meters	Study area lighter in tone than adjacent areas
e	5 meters	18 meters	13 meters	Study area lighter in tone than adjacent areas
f	5 meters	14 meters	9 meters	Study area lighter in tone than adjacent areas
g	5 meters	15 meters	10 meters	Study area lighter in tone than adjacent areas
h	5 meters	27 meters	22 meters	Study area characterized by a "rippled" texture
i	5 meters	20 meters	15 meters	Study area characterized by a "rippled" texture
j	5 meters	24 meters	19 meters	Study area lighter in tone than adjacent areas
k	3 meters	8 meters	5 meters	Study area lighter toned, also has rippled texture

TABLE A3. (continued)

STUDY AREA	AVERAGE WATER DEPTH STUDY AREA	AVERAGE WATER DEPTH ADJACENT AREAS	WATER DEPTH DIFFERENCE	STUDY AREA COMPARISON WITH ADJACENT AREAS
l	1 meter	6 meters	5 meters	Study area ligher toned than adjacent areas
m	3 meters	8 meters	5 meters	Study area lighter toned than adjacent areas
n	3 meters	12 meters	9 meters	Study area lighter toned than adjacent areas
o	3 meters	18 meters	15 meters	Study area lighter toned than adjacent areas
p	6 meters	13 meters	7 meters	Study area lighter toned, with rippled texture
q	7 meters	16 meters	9 meters	Study area lighter toned
r	8 meters	22 meters	13 meters	Study area lighter toned with rippled texture
s	5 meters	15 meters	10 meters	Study area lighter toned with rippled texture
t	11 meters	29 meters	18 meters	Study area lighter toned with rippled texture
u	8 meters	39 meters	31 meters	Study area lighter toned
v	9 meters	16 meters	7 meters	Study area lighter toned
w	9 meters	38 meters	27 meters	Study area lighter toned with rippled texture

TABLE A3. (continued)

STUDY AREA	AVERAGE WATER DEPTH STUDY AREA	AVERAGE WATER DEPTH ADJACENT AREAS	WATER DEPTH DIFFERENCE	STUDY AREA COMPARISON WITH ADJACENT AREAS
x	6 meters	20 meters	14 meters	Study area lighter toned than adjacent areas
y	11 meters	11 meters	0 meters	Study area has rippled texture
z	60 meters	60 meters	0 meters	Internal wave packets present
aa	120 meters	120 meters	0 meters	Internal wave packets present
bb	37 meters	37 meters	0 meters	Narrow line of light tone return
cc	17 meters	29 meters	12 meters	Study area has narrow band of light tone compared to adjacent areas
dd	23 meters	23 meters	0 meters	Study area lighter toned than adjacent areas
ee	37 meters	37 meters	0 meters	A line of sharp contrast exists where a lighter toned line follows an approximate 20 fathoms (37 meters) contour
ff	11 meters	41 meters	30 meters	Study area is lighter toned than adjacent areas
gg	3 meters	15 meters	12 meters	Study area lighter toned than adjacent areas
hh	3 meters	14 meters	14 meters	Study area lighter toned than adjacent areas

TABLE A3. (concluded)

STUDY AREA	AVERAGE WATER DEPTH		WATER DEPTH DIFFERENCE	STUDY AREA COMPARISON WITH ADJACENT AREAS
	STUDY AREA	ADJACENT AREAS		
ii	3 meters	12 meters	9 meters	Study area has a rippled texture
jj	1 meter	6 meters	5 meters	Study area lighter toned than adjacent areas
kk	1 meter	8 meters	7 meters	Study area lighter toned than adjacent areas
ll	20 meters	20 meters	0 meters	Study area has a rippled texture
mm	1 meter	8 meters	7 meters	Study area lighter toned than adjacent areas
nn	36 meters	50 meters	14 meters	Study area darker toned than adjacent areas
oo	46 meters	73 meters	26 meters	Study area darker toned than adjacent areas
pp	27 meters	46 meters	19 meters	Study area darker toned than adjacent areas
qq	73 meters	73 meters	0 meters	light, narrow band
rr	73 meters	73 meters	0 meters	light, narrow band
ss	13 meters	33 meters	20 meters	Study area darker than adjacent area
tt	24 meters	38 meters	14 meters	Study area darker than adjacent area
uu	40 meters	40 meters	0 meters	Study area darker than adjacent area

TABLE A4. BATHYMETRIC CORRELATION FOR SITE D, SUB-SITE 1, THAMES ESTUARY, SEASAT REV. 762

STUDY AREA	AVERAGE WATER DEPTH		WATER DEPTH DIFFERENCE	STUDY AREA COMPARISON WITH ADJACENT AREAS
	STUDY AREA	ADJACENT AREAS		
a	1.5 meters*	14 meters	12 meters	Study area very darkly toned compared to adjacent areas
b	1.5 meters*	14 meters	12 meters	Study area very darkly toned compared to adjacent areas
c	1.5 meters*	17 meters	15 meters	Study area very darkly toned compared to adjacent areas
d	2 meters	15 meters	13 meters	Study area has a darker tone compared to adjacent areas
e	2 meters*	16 meters	14 meters	Study area has a very much darker tone compared to adjacent areas
f	2 meters	15 meters	13 meters	Study area has a darker tone compared to adjacent areas
g	1.5 meters*	7 meters	5 meters	Study area has a darker tone compared to adjacent areas
h	23 meters	14 meters	9 meters	Study area has a lighter tone compared to adjacent areas
i	22 meters	4 meters	18 meters	Study area has a lighter tone compared to adjacent areas
j	1 meter*	8 meters	7 meters	Study area has a darker tone compared to adjacent areas

TABLE A4 (continued)

STUDY AREA	AVERAGE WATER DEPTH STUDY AREA	AVERAGE WATER DEPTH ADJACENT AREAS	WATER DEPTH DIFFERENCE	STUDY AREA COMPARISON WITH ADJACENT AREAS
k	27 meters	8 meters	19 meters	Study area has a lighter tone compared to adjacent areas
l	6 meters	1 meter	5 meters	Study area has a ligher tone compared to adjacent areas
m	11 meters	2 meters	9 meters	Study area has a lighter tone compared to adjacent areas
n	15 meters	8 meters	7 meters	Study area has a lighter tone compared to adjacent areas
o	12 meters	16 meters	4 meters	Study area has a darker tone than adjacent areas
p	2 meters*	20 meters	18 meters	Study area has a darker tone than adjacent areas
q	18 meters	9 meters	9 meters	Study area has a darker tone than adjacent areas
r	15 meters	20 meters	5 meters	Study area has a darker tone than adjacent areas
s	17 meters	10 meters	7 meters	Study area has a lighter tone than adjacent areas
t	1 meters*	7 meters	6 meters	Study area has a darker tone than adjacent areas
u	5 meters	11 meters	6 meters	Study area has a darker tone than adjacent areas

TABLE A4 (concluded)

STUDY AREA	AVERAGE WATER DEPTH STUDY AREA	AVERAGE WATER DEPTH ADJACENT AREAS	WATER DEPTH DIFFERENCE	STUDY AREA COMPARISON WITH ADJACENT AREAS
v	0 meters*	9 meters	9 meters	Study area is very much brighter than adjacent areas
w	0 meters*	, meters	7 meters	Study area is very much brighter than adjacent areas
x	0 meters*	9 meters	9 meters	Study area is very much brighter than adjacent areas
y	0 meters*	6 meters	6 meters	Study area is very much brighter than adjacent areas
z	0 meters*	6 meters	6 meters	Study area is very much brighter than adjacent areas
aa	0 meters*	13 meters	13 meters	Study area is very much brighter than adjacent areas
bb	1 meter*	15 meters	14 meters	Study area is very much brighter than adjacent areas
cc	0 meters*	7 meters	7 meters	Study area has a darker tone than adjacent areas
dd	15 meters	18 meters	3 meters	Study area has a darker tone than adjacent areas

*Study area might contain portions of an exposed sand or mud bank.

TABLE A5. BATHYMETRIC CORRELATION FOR SITE D, SUB-SITE 2, ENGLISH CHANNEL, SEASAT REV. 762

STUDY AREA	AVERAGE WATER DEPTH		WATER DEPTH DIFFERENCE	STUDY AREA COMPARISON WITH ADJACENT AREAS
	STUDY AREA	ADJACENT AREAS		
a	9 meters	40 meters	31 meters	Study area has a striped pattern, where one stripe is darker toned than the adjacent area, and the second band is lighter toned
b	22 meters	35 meters	13 meters	Same striped pattern, with study area having a rippled texture
c	7 meters	38 meters	31 meters	Same striped pattern, with study area having a rippled texture
d	6 meters	30 meters	24 meters	Same striped pattern, with study area having a rippled texture
e	6 meters	30 meters	24 meters	Same striped pattern, with study area having a rippled texture
f	8 meters	25 meters	17 meters	Same striped pattern, with study area having a rippled texture

APPENDIX B

GEOMETRIC CORRECTION OF SEASAT SAR DATA

APPENDIX B

GEOMETRIC CORRECTION OF DIGITAL SEASAT SAR DATA

In order to assess how closely the relative radar backscatter measurements present on the JPL digital tapes correlate to bathymetric information, it was first necessary to geometrically correct the JPL data in the range direction. The backscatter scans were made by averaging five lines of pixels across the range direction. The backscatter scans were then geometrically corrected using the algorithm of Shuchman, et a., 1978. In this algorithm, G_R (ground range from nadir) is expressed as:

$$G_R = \rho_e \, a \cos \left[\rho_e^2 + \frac{(\rho_e + a)^2 - S_R^2}{2 \rho_e (\rho_e + a)} \right] \qquad (1)$$

where:

ρ_e = radius curvature of the earth

a = altitude of spacecraft

S_R = slant range

This algorithm was tested using a portion of SEASAT Revolution 880 (see Figure 1). A transect was taken through Nantucket Island through the city of Nantucket. By making a grey-map of Nantucket Island, it was possible to locate where the transect crossed the two shorelines, and the pixel numbers of these points were recorded. From these pixel numbers, it was then possible to locate their respective ground range distances on a computer printout from a program based on Equation (1).

By subtracting the two ground range distances, an estimate of the transect distance over land was produced. This estimate was 17,005 meters. The transect was next located on NOAA Chart #13237 (Nantucket Sound and Approaches). This estimated distance for the transect on the chart was 17,040 meters. The difference between the two estimates was .2%. Therefore, the algorithm was judged to be accurate enough for the purposes of backscatter-bathymetry comparisons.

Figure B1. Transect Location, Revolution 880.